





RESEARCH ARTICLE
10.1029/2021MS002849

Algorithmic Differentiation for Sensitivity Analysis in Cloud Microphysics

M. Hieronymus¹ , M. Baumgartner¹, A. Miltenberger² , and A. Brinkmann¹

¹Zentrum für Datenverarbeitung, Johannes Gutenberg University Mainz, Mainz, Germany, ²Institute for Atmospheric Physics, Johannes Gutenberg University Mainz, Mainz, Germany

Key Points:

- Quantification of multi-parameter uncertainty of cloud microphysical evolution of WCB trajectories using algorithmic differentiation
- Uncertainty at every time step derived with algorithmic differentiation representative for key uncertainty over at least 30 min intervals
- Parameterization of CCN activation, diameter size, and fall velocity of hydrometeors have the largest mean impact on water vapor contents

Supporting Information:

Supporting Information may be found in the online version of this article.

Correspondence to:

M. Hieronymus,
mhieronymus@uni-mainz.de

Citation:

Hieronymus, M., Baumgartner, M., Miltenberger, A., & Brinkmann, A. (2022). Algorithmic differentiation for sensitivity analysis in cloud microphysics. *Journal of Advances in Modeling Earth Systems*, 14, e2021MS002849. <https://doi.org/10.1029/2021MS002849>

Received 26 SEP 2021
Accepted 27 JUN 2022

Author Contributions:

Conceptualization: M. Hieronymus, M. Baumgartner, A. Miltenberger
Data curation: M. Hieronymus
Formal analysis: M. Hieronymus
Investigation: M. Hieronymus, M. Baumgartner, A. Miltenberger
Methodology: M. Hieronymus
Software: M. Hieronymus
Supervision: M. Baumgartner, A. Miltenberger
Validation: M. Hieronymus
Visualization: M. Hieronymus

© 2022 The Authors. Journal of Advances in Modeling Earth Systems published by Wiley Periodicals LLC on behalf of American Geophysical Union. This is an open access article under the terms of the [Creative Commons Attribution License](https://creativecommons.org/licenses/by/4.0/), which permits use, distribution and reproduction in any medium, provided the original work is properly cited.

Abstract The role of clouds for radiative transfer, precipitation formation, and their interaction with atmospheric dynamics depends strongly on cloud microphysics. The parameterization of cloud microphysical processes in weather and climate models is a well-known source of uncertainties. Hence, robust quantification of this uncertainty is mandatory. Sensitivity analysis to date has typically investigated only a few model parameters. We propose algorithmic differentiation (AD) as a tool to detect the magnitude and timing at which a model state variable is sensitive to any of the hundreds of uncertain model parameters in the cloud microphysics parameterization. AD increases the computational cost by roughly a third in our simulations. We explore this methodology as the example of warm conveyor belt trajectories, that is, air parcels rising rapidly from the planetary boundary layer to the upper troposphere in the vicinity of an extratropical cyclone. Based on the information of derivatives with respect to the uncertain parameters, the ten parameters contributing most to uncertainty are selected. These uncertain parameters are mostly related to the representation of hydrometeor diameter and fall velocity, the activation of cloud condensation nuclei, and heterogeneous freezing. We demonstrate the meaningfulness of the AD-estimated sensitivities by comparing the AD results with ensemble simulations spawned at different points along the trajectories, where different parameter settings are used in the various ensemble members. The ranking of the most important parameters from these ensemble simulations is consistent with the results from AD. Thus, AD is a helpful tool for selecting parameters contributing most to cloud microphysics uncertainty.

Plain Language Summary The formation of clouds is determined by processes that act on smaller scales than weather prediction models can resolve. Consequently, a parameterization with typically hundreds of parameters is constructed to determine the effects of these processes on the resolved larger scales. These parameters are a well-known source of uncertainty in weather and climate models. Classical attempts to quantify this uncertainty are typically limited to a few parameters. We propose algorithmic differentiation (AD) as a tool to detect parameters with the largest impact for any of the hundreds of parameters on multiple model state variables at every time step in our simulation. This increases the computational cost by roughly a third. The relevance of the AD-estimated impact is demonstrated by comparing the AD results with ensemble simulations, where different parameter settings are used in the various ensemble members. The ranking of the most important parameters from these ensemble simulations is consistent with the results from AD. Thus, AD is a helpful tool to identify parameters objectively that contribute most to uncertainty in cloud parameterizations.

1. Introduction

Numerical models of the atmosphere such as numerical weather prediction (NWP) models or climate models both face the challenge of properly resolving physical processes on all relevant spatial and temporal scales. These include many processes operating at scales smaller than the grid-spacing of the models, for example, cloud physics, which therefore cannot be explicitly represented. As a consequence, all of these subgrid processes need to be parameterized, that is, their effect on the resolved scales needs to be modeled. In the context of cloud modeling, a good parameterization is crucial to capture the impact of clouds on radiation, the hydrological cycle, and dynamics. Since parameterizations are usually not rigorously derived from first principles, they contain ad-hoc assumptions or rely on the fitting of observed data. Parameters are introduced which are uncertain to some degree or even represent artificial processes without a strict physical interpretation. Consequently, it is important to assess the impact of this so-called parametric uncertainty, that is, the degree to which the uncertainty in a specific

Writing – original draft: M. Hieronymus
Writing – review & editing: M. Baumgartner, A. Miltenberger

parameter value choice influences the model result. There are several attempts to understand the sensitivity of parameters in the literature.

The probably most straightforward way to investigate parametric uncertainty is to pick a specific parameter deemed to be particularly uncertain or important and to conduct a number of simulations with different choices for the numeric value of this parameter. Morris (1991) describes plans for independent random sampling using a sampling matrix to assess the impact of single parameters with varying perturbation with few simulations. Another method described there uses Latin hypercube sampling, which samples the uncertain parameter space while ensuring maximum distance between different parameter combinations. Finally, he describes the usage of cluster sampling, which considers more than one effect during a simulation as long as these effects do not strongly affect each other. Specific examples in the context of cloud modeling are the studies by Igel and van den Heever (2017a); Igel and van den Heever (2017b), who considered a parameter describing the width of the droplet size distribution in shallow cumulus clouds. By varying this parameter, they found that its value significantly affects the simulated clouds.

In the context of cloud microphysics, statistical sampling techniques were used, for example, by Johnson et al. (2015), who used a maximin Latin hypercube design, which maximizes the minimum distance between points, to obtain a statistically meaningful sample of a multidimensional parameter space. Based on the sampling with complex model simulations, they construct a statistical emulator, being a surrogate representation using the Gaussian process as initially proposed by Oakley and O'Hagan (2004). That allows a variance-based analysis of the impact of several (input) parameters on the model output. Although emulators can be very effective, they often rely on prior knowledge, which might not always be available, or on assuming specific distributions of the parameters, for example, a Gaussian distribution. Also, in the case of high dimensional parameter spaces, many complex model simulations are still required. Following the idea of applying emulators, Wellmann et al. (2018) trained emulators for deep convective clouds using idealized cloud-resolving model simulations in order to assess the parameter sensitivity, and Regayre et al. (2014) investigated the sensitivity of radiative properties of clouds to aerosols in a global climate model. These approaches investigate only a single parameter or a small number (in the order of 10) of parameters due to the large number of computationally expensive simulations required.

An entirely different approach, which incorporates uncertainty into the model itself rather than quantifying it in additional experiments, is outlined in Chertock et al. (2019). A stochastic Galerkin method is employed to solve the Navier-Stokes equations coupled to a cloud model. One carefully chosen parameter is assumed to be stochastic, and the resulting distribution of all model state variables is estimated as a solution to the model, that is, including their mean and standard deviation. Although this approach is extremely powerful, it becomes highly expensive to include several independent stochastic variables. Computing the statistical distribution of the model variables in response to assumed distributions of model parameters provides a complete and desirable treatment of parametric uncertainty. However, the stochastic Galerkin approach is, at the moment, only feasible for a very small number of stochastic parameters.

Buizza et al. (1999) introduced Stochastically Perturbed Parametrization Tendencies (SPPT; refined by Palmer et al. (2009)). SPPT pools the uncertainty of several processes and uses spatio-temporally correlated multiplicative noise for perturbing parametrized tendencies. Since tendencies are not independent of each other, the perturbation must be applied to the sum of the parametrized tendencies. This is not ideal since all processes are perturbed using the same error characteristics, assuming a perfect correlation with each other (Leutbecher et al., 2017). Christensen et al. (2017) generalized this approach such that six physics processes are perturbed independently (iSPPT). This increases the variance of ensemble simulations, and one can estimate the impact of distinct processes. These benefits come at a cost: perturbing parameters independently increases the dimensionality of the phase space, and parametrization schemes are assumed to be perfectly uncorrelated. Grouping similar and correlated processes and perturbing those is an intermediate approach between SPPT and iSPPT.

Ollinaho et al. (2017) developed the Stochastically Perturbed Parametrizations (SPP) scheme that can be applied complementary to SPPT. In SPP, one adds stochastic noise that varies in time and space on a process-level. The perturbations are independent to each of the parameters, but the perturbation patterns contain a spatial and temporal correlation that evolve as a first order auto-regressive process. Lang et al. (2021) revised SPP by perturbing additional parameters and modifying the probability distributions used in the scheme. In this revised version, 27 parameters are perturbed with six of them in the cloud scheme. The medium-range forecast scores and the

computational cost are similar to SPPT, but the degree of freedom remains higher than in SPPT. Therefore, tuning SPP is still more challenging.

Since existing approaches are currently only capable of exploring the sensitivity of model simulations to a very limited set of parameters and given the overall number of parameters entering complex parameterization schemes, the main question remains: how can we effectively find the most sensitive parameters? To answer this question, we explore the use of algorithmic differentiation (AD; also known as automatic differentiation), which was used for the first time in the context of cloud schemes for idealized trajectories and a simple warm-rain microphysics scheme by Baumgartner et al. (2019).

A thorough explanation of AD is given by Griewank and Walther (2008). In a nutshell, AD considers a computer program as a long concatenation of elementary operations which are differentiable. As a consequence of the chain rule, the whole program is differentiable. The AD technique allows to compute its derivatives with a linear increase of the execution time depending on the number of output or input parameters. Based on the computed derivatives, one can rank model parameters by their direct and indirect impact for a given model trajectory during run time without further work. Bischof et al. (1996) demonstrated a sensitivity analysis with the MM5 mesoscale modeling system, where a tangent linear model, a model to describe the linearized evolution of errors or perturbations, is created with AD to assess the impact of adding additional observations to the initial temperature field. Kim et al. (2006) applied AD to the Community Climate System Model (CCSM), where a sensitivity-enhanced simulation was investigated to identify important thermodynamic and dynamic parameters and to provide a tuning guide, which demonstrated how easy a multivariate sensitivity analysis can be done with AD in Fortran 77. AD is a tool that is often used outside of sensitivity analysis. A prominent example of optimizing parameters of a model via gradient descent is machine learning (e.g., Paszke et al., 2019). AD may be used for any maximization of an objective function using gradient descent or Newton's method (Margossian, 2019) or other algorithms where gradients are needed, such as in fluid dynamics, where differentiating fixed point iterations may be necessary, and AD is used to decrease the memory requirement (Schlenkrich et al., 2008).

In this study, we use AD to gain insight into the sensitivity of the cloud microphysical evolution of air parcels with hundreds of uncertain model parameters and 23 prognostic cloud state variables in a two-moment cloud microphysics parameterization. Applying AD at every time step increases the execution time by roughly a third in our simulation. We use warm conveyor belt (WCB) trajectories as a case study, which are of special interest due to their impact on large-scale precipitation patterns, the hydrometeor, and potential vorticity distribution in a wide region (Madonna et al., 2014). The formulation of the microphysics is based on the cloud scheme as implemented in the Icosahedral Nonhydrostatic (ICON; Zängl et al. (2015)) model or the COnsortium for Small-scale MOdeling model (COSMO; Baldauf et al. (2011)) and was originally presented in Seifert and Beheng (2006a); Seifert and Beheng (2006b). We use this scheme to compute the sensitivity of multiple state variables for hundreds of model parameters along trajectories to identify the key parameters that have the biggest impact on each model state variable. We further evaluate the relevance of gradients for each time step for the longer term (i.e., about the next half hour) cloud microphysical evolution.

The outline of this study is as follows: in Section 2, we give an introduction to AD, we present the trajectories used, and we describe the model for the cloud microphysical evolution. Section 3 contains the methods used to quantify sensitivities using either AD or ensemble simulations for comparison. We give an example of how sensitivities change over time in Section 4, and we discuss the identified key parameters. Section 5 dissects the relevance of sensitivities for longer time evolution and gives an example of a possible pitfall when applying algorithmic differentiation. We close this study with a conclusion and suggestions for future work in Section 6.

Table 1 gives an overview of the model state variables and sedimentation rates and their notation, and Table 2 lists the ten most important parameters identified by AD for each model state variable. Table A1 shows the identified most important parameters with a description and the model state variable with their largest impact. Table 3 shows the correlation between AD-estimated and ensemble-estimated deviations for mass densities, whereas Table B1 shows the correlation for all model state variables and sedimentation rates.

Table 1
An Overview of the 23 Model State Variables for Which Sensitivities Are Calculated

Model state variable	Notation
Water vapor mass density	Q_{vapor}
Cloud droplets mass density	Q_{cloud}
Rain droplets mass density	Q_{rain}
Graupel mass density	Q_{graupel}
Hail mass density	Q_{hail}
Ice mass density	Q_{ice}
Snow mass density	Q_{snow}
Cloud droplet number density	N_{cloud}
Rain droplet number density	N_{rain}
Graupel number density	N_{graupel}
Hail number density	N_{hail}
Ice crystal number density	N_{ice}
Snowflake number density	N_{snow}
Rain droplet number density (sedimentation)	$N_{\text{rain,out}}$
Graupel number density (sedimentation)	$N_{\text{graupel,out}}$
Hail number density (sedimentation)	$N_{\text{hail,out}}$
Ice crystal number density (sedimentation)	$N_{\text{ice,out}}$
Snowflake number density (sedimentation)	$N_{\text{snow,out}}$
Rain droplets mass density (sedimentation)	$Q_{\text{rain,out}}$
Graupel mass density (sedimentation)	$Q_{\text{graupel,out}}$
Hail mass density (sedimentation)	$Q_{\text{hail,out}}$
Ice mass density (sedimentation)	$Q_{\text{ice,out}}$
Snow mass density (sedimentation)	$Q_{\text{snow,out}}$

Note. The word “sedimentation” refers to the mass and number densities that sediment out of the simulated air parcel.

2. Data and Methods

In the following, we explain the principles of algorithmic differentiation, the different modes that can be used, and the limits of this method to evaluate gradients. We give an overview of the convective trajectories that have been identified for the extratropical cyclone Vladiana. Finally, we describe some key equations of the microphysical model.

2.1. Algorithmic Differentiation

Algorithmic Differentiation (AD) is a technique to compute derivatives of a given computer code. Once implemented, the computation of the derivatives is achieved automatically alongside the usual run of the computer code, hence the computation of the derivatives is automatic (Griewank & Walther, 2008). The derivative of the program may also be seen as the sensitivity of the output to an input. Since any computer code is a concatenation of simple differentiable functions, so-called “elemental operators,” such as addition, multiplication, trigonometric functions, or exponentials, the chain rule implies that the whole code, and hence the model it represents, is differentiable. For the subsequent description of AD, we follow the notation and exposition by Sagebaum et al. (2019). Given a theoretical model $\mathcal{M}^* : X \subset \mathbb{R}^{n_{\text{in}}} \rightarrow Y \subset \mathbb{R}^{n_{\text{out}}}$ with n_{in} input (or model) parameters and n_{out} output (or model state) variables, we can formally write its implementation \mathcal{M} as a concatenation of elemental mappings Φ_i

$$y = \mathcal{M}(x) = I_{V,Y} \circ \Phi_k \circ \Phi_{k-1} \circ \dots \circ \Phi_2 \circ \Phi_1 \circ I_{X,V}(x), \quad (1)$$

with $U \subset \mathbb{R}^l$ the space of the intermediate values, $V = X \times U \times Y$ the space of the program evaluation $\Phi_i(v)$, and $k = l + n_{\text{out}}$ the number of operations. Each elemental mapping has the form $\Phi_i(v) = (v_1, \dots, v_{n_{\text{in}}+i-1}, \phi_i(v), 0, \dots, 0)$, where $\phi_i : V \rightarrow \mathbb{R}$ is an elemental operator. The matrix $I_{X,V} \in \mathbb{R}^{(n_{\text{in}}+k) \times n_{\text{in}}}$ projects an input vector onto the first n_{in} components of an $(n_{\text{in}} + k)$ vector, and $I_{V,Y} \in \mathbb{R}^{n_{\text{out}} \times (n_{\text{in}}+k)}$ projects an $(n_{\text{in}} + k)$ vector onto its last n_{out} components for the final output. It is important to note that the resulting gradients are given by the implemented model \mathcal{M} and not by the underlying theoretical model \mathcal{M}^* . This implies several dependencies for the derivatives: they may depend on the numerical methods, the time step size, the machine precision,

the evolution of the model, that is, each set of initial parameters may result in different gradients. Baumgartner et al. (2019) give an example of different temporal evolutions of the derivative with different time steps in their Figure 4. Furthermore, parameters in a model used solely as thresholds, that is, as an argument in an if-clause, may have a big impact on the model output by changing the control flow, but a gradient cannot be determined. As an example, consider the following function:

$$y(x, a, b) = \begin{cases} 2 \cdot x & \text{for } x \leq a \\ x^b & \text{for } x > a \end{cases} \quad (2)$$

In this example, a is a threshold, which would be implemented with an if-clause such as `if (x <= a)`. A gradient $\partial y / \partial a$ would yield zero for both cases, even though changing a can potentially change the evolution of the model. In addition, a gradient $\partial y / \partial b$ is always zero if the latter case does not occur during the simulation, which demonstrates the dependency of gradients on the progression of the model. If the exponent in Equation 2 was a instead of b , then AD would yield a gradient for $\partial y / \partial a$, but only for the case $x > a$. Another caveat is when a gradient becomes a complex number, which might not be handled by an AD tool, and where the interpretation is not straightforward if the input and output are restricted to real numbers. We discuss this aspect with an example in Appendix C.

Table 2
The top 10 Parameters for Each Model State Variable y_s

Model state variable	Top 10 parameters
Water Vapor Mass Density	$geo_{b,ice}, geo_{a,ice}, b_{ccn,4}, c_{ccn,4}, vel_{b,ice}$ $b_{ccn,1}, c_{ccn,1}, d_{ccn,4}, a_{ccn,4}, geo_{b,graupel}$
Cloud Mass Density	$b_{ccn,1}, b_{ccn,4}, c_{ccn,1}, c_{ccn,4}, d_{ccn,4}$ $d_{ccn,1}, a_{ccn,4}, geo_{b,graupel}, k_r, a_{ccn,1}$
Rain Mass Density	$geo_{b,rain}, \alpha_{rain}, \beta_{rain}, vel_{b,rain}, z^{-1}$ $b_{ccn,1}, b_{ccn,4}, c_{ccn,1}, c_{ccn,4}, geo_{a,rain}$
Graupel Mass Density	$vel_{b,rain}, vel_{b,graupel}, geo_{b,rain}, geo_{b,graupel}, z^{-1}$ $vel_{a,rain}, p_{sat,melt}, v_{graupel,sedi,max}, geo_{a,rain}, vel_{a,graupel}$
Hail Mass Density	$\mu_{rain}, geo_{b,rain}, x_{rain,min,frz}, x_{min,rain}, D_{rainfrz,ig}$ $geo_{a,rain}, \nu_{rain}, z^{-1}, \beta_{rain}, k_r$
Ice Mass Density	$geo_{b,ice}, d_{ccn,4}, a_{ccn,4}, vel_{b,rain}, d_{ccn,1}$ $a_{ccn,1}, vel_{b,ice}, z^{-1}, v_{ice,sedi,max}, geo_{a,ice}$
Snow Mass Density	$\mu_{rain}, geo_{b,snow}, a_{HET}, vel_{b,graupel}, geo_{b,rain}$ $geo_{b,graupel}, vel_{b,rain}, vel_{b,snow}, p_{sat,melt}, vel_{a,graupel}$
Cloud Droplet Particle Density	$b_{ccn,4}, c_{ccn,4}, b_{ccn,1}, c_{ccn,1}, d_{ccn,4}$ $a_{ccn,4}, d_{ccn,1}, a_{ccn,1}, d_{ccn,3}, b_{ccn,3}$
Rain Droplet Particle Density	$b_{ccn,1}, b_{ccn,4}, c_{ccn,1}, c_{ccn,4}, d_{ccn,4}$ $d_{ccn,1}, \alpha_{rain}, \beta_{rain}, a_{ccn,4}, a_{ccn,1}$
Graupel Particle Density	$geo_{b,rain}, geo_{b,ice}, \mu_{rain}, vel_{b,graupel}, vel_{b,rain}$ $geo_{b,snow}, D_{rainfrz,gh}, geo_{a,rain}, a_{HET}, vel_{b,ice}$
Hail Particle Density	$\mu_{rain}, x_{rain,min,frz}, x_{min,rain}, geo_{b,rain}, D_{rainfrz,ig}$ $geo_{a,rain}, a_{HET}, b_{HET}, \alpha_{rain}, vel_{b,rain}$
Ice Particle Density	$d_{ccn,4}, a_{ccn,4}, d_{ccn,1}, a_{ccn,1}, vel_{b,ice}$ $c_{ccn,4}, d_{ccn,2}, c_{ccn,1}, T_{mult,max}, geo_{b,ice}$
Snow Particle Density	$geo_{b,rain}, \mu_{rain}, geo_{b,ice}, a_{HET}, geo_{b,snow}$ $D_{rainfrz,gh}, geo_{a,rain}, vel_{b,ice}, vel_{b,rain}, geo_{a,ice}$

Note. The parameters are sorted by the associated $MSD_{pred}(y_s)$. Cloud droplets are most sensitive to parameters related to CCN activation (see Equation (13)), whereas frozen hydrometeors are mostly sensitive to the geometry of particles.

Table 3
Spearman's Rank Correlation for AD-Estimated Deviation MSD_{pred} and Ensemble-Estimated Deviation MSD for Every Mass Density State Variable

Model state variable y_s	$r(y_s)$ without zero sensitivities	$r(y_s)$
Water Vapor Mass Density	0.863	0.889
Cloud Mass Density	0.927	0.904
Rain Mass Density	0.901	0.868
Graupel Mass Density	0.900	0.845
Hail Mass Density	0.906	0.818
Ice Mass Density	0.924	0.884
Snow Mass Density	0.864	0.815
All Together	0.887	0.543

Note. The second column uses only those parameters x_p , where AD estimated a sensitivity above zero, that is, where $MSD_{pred}(y_s, x_p) > 0$.

Two important questions can be addressed using AD:

1. To which input is a given model state variable y_s most sensitive?
2. Which output does the model parameter x_p influence the most?

$$\frac{dM}{dx} \quad (3)$$

From a mathematical point of view, both questions can be answered using the Jacobian of the model \mathcal{M} . The strength of AD becomes eminent by noting that AD computes the effect of the program's Jacobian on a given vector without forming the Jacobian explicitly. This is the benefit of AD since the Jacobian can require large amounts of memory with many input and output variables. Furthermore, the evaluation for desired gradients can be optimized, reducing any possible overhead that might come with different techniques for evaluating the Jacobian implicitly. The obtained gradients are in machine precision, avoiding round-off problems as in, for example, finite-difference

methods. AD calculates in one sweep either the partial derivatives of all outputs with respect to one input, called forward mode, or the partial derivatives of one output with respect to all inputs, called backward mode. The first question posed above, that is, that regarding the biggest impact on a given output variable, refers to the backward mode of AD, which is recommended when more input than output parameters are present ($n_{in} > n_{out}$). The second question corresponds to the forward mode recommended for $n_{out} > n_{in}$. The difference between those modes becomes clear by looking at the calculation of the directional derivatives for the forward mode suitable for each direction $\hat{x} \in \{e_1, e_2, \dots, e_{n_{in}}\}$:

$$\dot{y} = \frac{d\mathcal{M}}{dx}(x)\hat{x}, \quad (4)$$

where $x \in X$ is the vector of input variables (initial state or, in our case, model parameters), $y \in Y$ is the vector of output variables (in our case, the model state variables), and e_i denotes the standard unit vector in direction i . On the other hand, in the backward mode AD calculates the adjoint derivative for every adjoint direction, denoted by $\bar{y} \in \{e_1, e_2, \dots, e_{n_{out}}\}$, via

$$\bar{x} = \frac{d\mathcal{M}}{dx}(x)^T \bar{y}. \quad (5)$$

The number of necessary calculations for the forward mode depends on the number of input variables n_{in} , whereas the backward mode scales with the number of output variables n_{out} . In our model, we are going to analyze 177 model parameters and their impact on 23 output parameters, such that $n_{in} = 177 \gg 23 = n_{out}$, and hence we use the backward mode. Applying AD increases the execution time of our simulations by roughly a third. We selected the parameters based on the model descriptions given by Seifert and Beheng (2001); Seifert and Beheng (2006a, 2006b), Seifert (2008), Phillips et al. (2008), Hallett and Mossop (1974), and Hande et al. (2016). Parameters that have an explicit dependency on other parameters have been excluded wherever possible and the impact of the latter is tracked instead. For example, Seifert and Beheng (2006a) describe a parameter $\bar{a}_{vent,n}$ (their Equation (88)) for calculating an averaged ventilation coefficient (their Equation (85)). This constant depends on the diameter-mass relation, the velocity-mass relation, and on the constants of the generalized Γ -distribution which are tracked instead. Resolving all dependencies is not feasible for all parameters, that is, coupled parameters whose values are tuned are tracked as they were independent. We discuss this in more detail in Section 3.1.

AD can be implemented via source transformation, that is, by parsing code with an external program to produce additional code that has statements for the forward or backward mode. Tapenade (Hascoet & Pascual, 2013) is such a tool written in Java for Fortran; some features for newer Fortran versions and C are also implemented. There is, however, a major drawback of source transformation: features from modern languages, such as classes or templates, which can make it easier to implement AD in a model, are not easily supported. A different approach is operator overloading, avoiding the aforementioned downside while maintaining similar execution speeds (see Hogan (2014) for the benefits of static polymorphism and expression templates used in operator overloading). In this case, an operator returns an expression template (Veldhuizen, 1995) rather than a (temporary) object, where lazy evaluation is used in order to create structures during compile time representing calculations that are only evaluated when needed. Rather than creating possibly multiple temporary objects to get the result stored in a single object, an expression graph is created, which a compiler can optimize, even ignoring the normal order of evaluation of a language. Polymorphism allows the treatment of different objects of different types but with the same base type as if they are of the same type using the same interface, such that different expression templates can be evaluated together. CoDiPack (Code Differentiation Package; Sagebaum et al., 2019) is a tool that uses this approach for C++, and we apply this tool to our simulations. The data layout used in CoDiPack creates a small memory footprint, and caching strategies of the processors can be applied. CoDiPack has been created for High Performance Computing environments and is used in simulation packages such as adFVM (Talnikar & Wang, 2019) or SU2 (Economou et al., 2016).

2.2. Trajectories From Warm Conveyor Belts

Warm conveyor belts (WCBs) are an important phenomenon of extra-tropical weather, since “the WCB represents a well-defined moist airflow at the leading edge of the trough, ascending from the boundary layer to the upper troposphere, and is regarded as the primary cloud- and precipitation-producing flow within extratropical

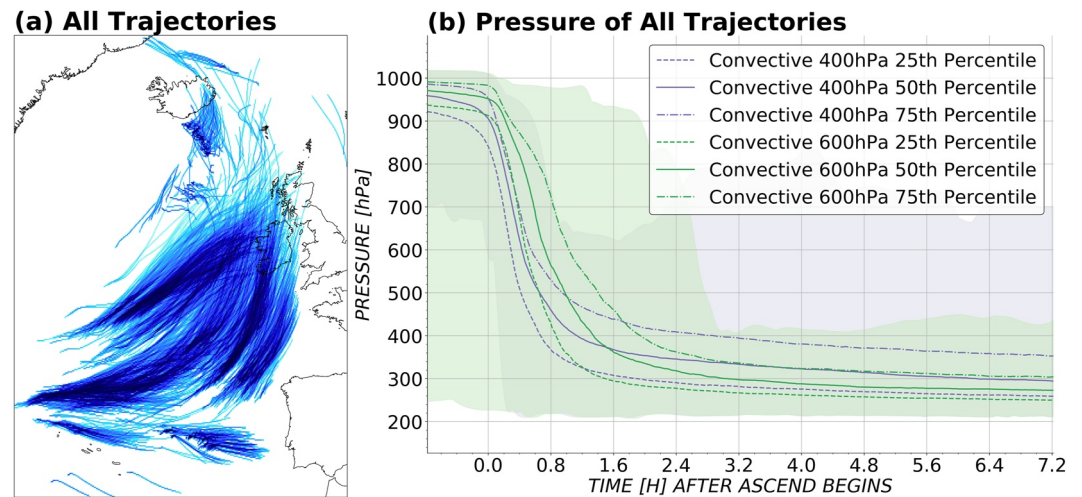


Figure 1. Overview of all convective trajectories with either a 400 hPa or 600 hPa ascent within one or three hours, respectively, in our data set. (a) The geographic location of all trajectories (over the North Atlantic Ocean). The blue shade represents the number of trajectories. (b) The evolution of parcel air pressure for different sets of trajectories relative to the onset of rapid ascent. The 75th percentile is dot-dashed, the 50th percentile (median) is a solid line, and the 25th percentile is dashed. The shading indicates the area between min and max pressure values at each time step.

cyclones” (Wernli, 1997). It is the strong ascent in the WCB that typically causes the formation of clouds and precipitation, which result in an increasing potential temperature (due to latent heating) and a decreasing specific humidity along the WCB (e.g., Madonna et al., 2014). The latent heating occurring during WCB ascent further has been demonstrated to affect the potential vorticity structure throughout the troposphere with direct implications for flow dynamics (e.g., Joos & Wernli, 2012). Hence, WCBs play an important role in the dynamics of extratropical cyclones and associated precipitation (e.g., Büeler & Pfahl, 2017). Case study investigations suggest that the details of the cloud microphysics scheme can matter for the resulting potential vorticity structure and thereby impact the larger scale dynamics (Joos & Forbes, 2016).

Considerations of the WCB ascent in convection-permitting simulations have highlighted the importance of embedded convection in WCBs. The different ascent rates in the “conventional” continuously and slantwise ascending WCB trajectories differ from those of trajectories experiencing rapid, convective lifting along segments of their ascent due to the embedded convection (e.g., Oertel et al., 2019). The ascent rates imply differences in the dominant cloud microphysical processes in the two sub-sets of WCB trajectories (e.g., Oertel et al., 2020), which makes both slantwise and convective ascending trajectories interesting test cases for themselves. It has further been suggested that slantwise ascending trajectories dominate the large-scale precipitation pattern, the hydrometeor, and potential vorticity distribution at large-scales, while trajectories with convective ascending segments have a bigger impact on surface precipitation rates (Oertel et al., 2019, 2020). Following the categorization introduced by Oertel et al. (2020), a WCB trajectory is considered slantwise if the 400 hPa and 600 Pa ascent times are between 1.5 to 3.5 hr and 6.5–22 hr, respectively. A WCB trajectory is convective if the fastest 400 hPa and 600 hPa ascent times are shorter than one hour and three hours, respectively. Due to their impact on cloud evolution and, therefore, various microphysical processes that occur in a short time, we here focus on convective WCB trajectories.

Trajectories are computed for the extratropical cyclone “Vladiana,” which developed from 22 to 25 Sep 2016 in the North Atlantic during the North Atlantic Waveguide and Downstream Impact Experiment field campaign (Schäfler et al., 2018). Figure 1a shows the convective WCB trajectories, and Figure 1b displays the evolution of pressure along these trajectories, that is, indicates the ascent rates of the air parcels. The simulation of the case-study we use here to derive trajectories was conducted with the COSMO model version 5.1 (Baldauf et al., 2011) following the model setup described by Oertel et al. (2020). In contrast to Oertel et al. (2020), we use the two-moment scheme by Seifert and Beheng (2006a) for representing cloud microphysics as described in Section 2.3. The trajectories have been computed with the COSMO online trajectory scheme (Miltenberger

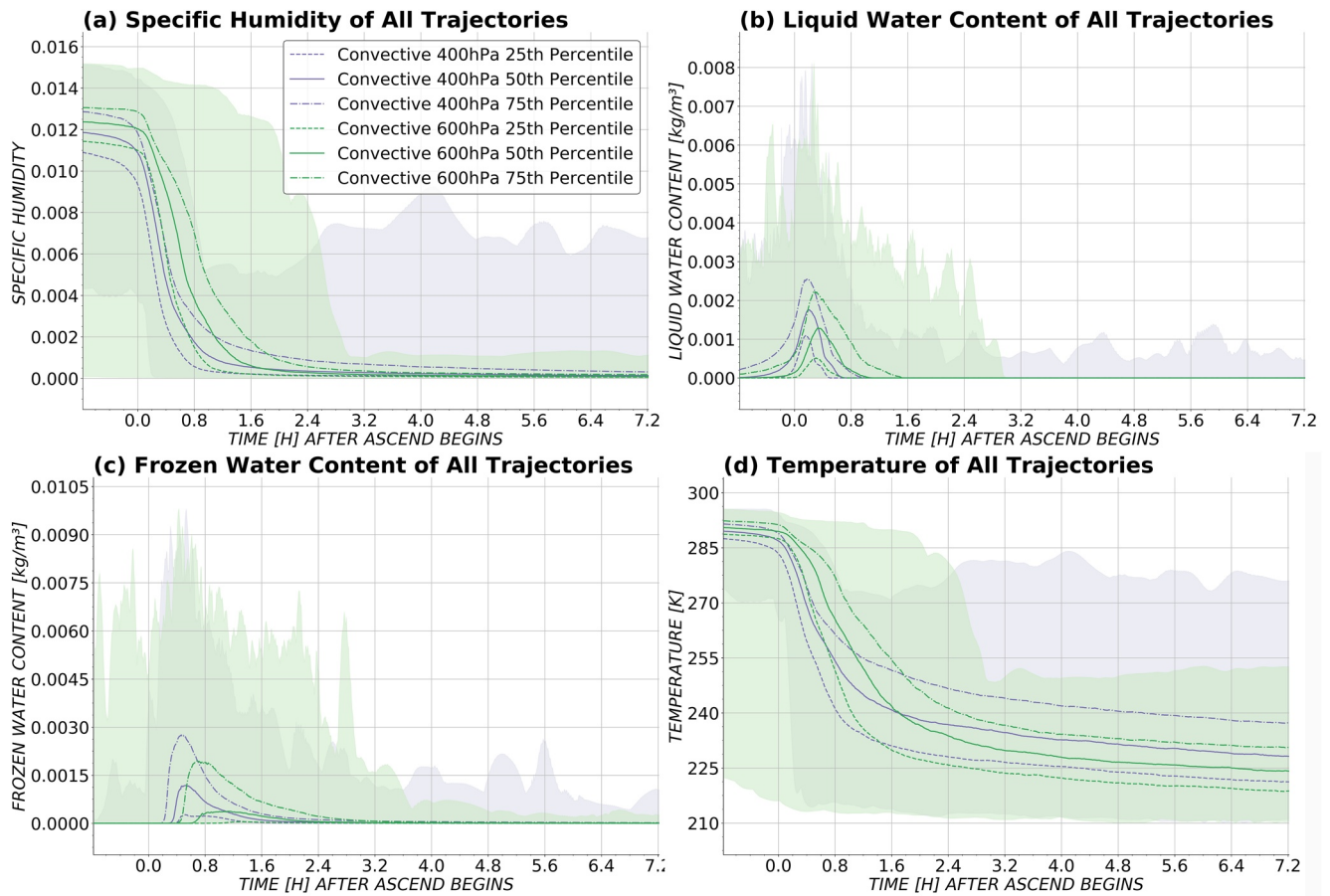


Figure 2. An overview of all convective trajectories with either a 400 hPa (purple) or 600 hPa (green) ascent within one or three hours, respectively, in our data set. We set the start time to the start of the ascent of the trajectories and show the 25th (dashed line), 50th (solid line), and 75th percentiles (dot-dashed lines). The shaded area enfolds the entire data region. (a) shows the specific humidity, (b) the sum of cloud and rain droplet mass densities, (c) the sum of snow, ice, graupel, and hail mass densities, and (d) the temperature.

et al., 2013). The positions of the trajectories are calculated from the resolved 3D wind field at every model time step, here 20 s. We use the same starting positions and times of the online trajectories as in Oertel et al. (2020).

Our data set consists of 2,199 convective trajectories where 2,036 trajectories ascend 400 hPa within one hour, and 1,240 trajectories ascend 600 hPa within three hours. These two categories are not mutually exclusive such that 1,077 trajectories fall into both categories. For each category, we computed three representative trajectories, that is, the 25th, 50th, and 75th percentile trajectory. Figure 1b shows the temporal evolution of pressure and Figure 2 that of the specific humidity (a), liquid water content (b), frozen water content (ice, snow, graupel, and hail) (c), and the temperature (d) along the convective trajectories. From these trajectories the thermodynamic conditions ($T(t)$, $p(t)$) and initial values ($Q_{\text{vapor}}(t = t_0)$, $Q_{\text{cloud}}(t = t_0)$, ...) are used to drive our box-model simulation.

2.3. Description of the Cloud Microphysics Model

We re-implemented the two-moment cloud microphysics, as described later in this section, in C++ in order to apply AD with the library CoDiPack. We use the thermodynamics from representative trajectories, that is, the 25th, 50th, and 75th percentile trajectories, of the COSMO simulation as drivers to get a realistic thermodynamic evolution of individual air parcels. Figure 3 depicts the workflow of the simulation. These selected thermodynamic air parcel trajectories, together with the parcel's initial specific humidity, are used for a recomputation of the cloud microphysical evolution using a box-model simulation. We apply the Runge-Kutta method of order four (Hairer & Wanner, 1996) for our cloud microphysics, whereas the default integration method for COSMO is the Runge-Kutta method of order three. Our choice is, in the worst case, as accurate as the COSMO variant in the

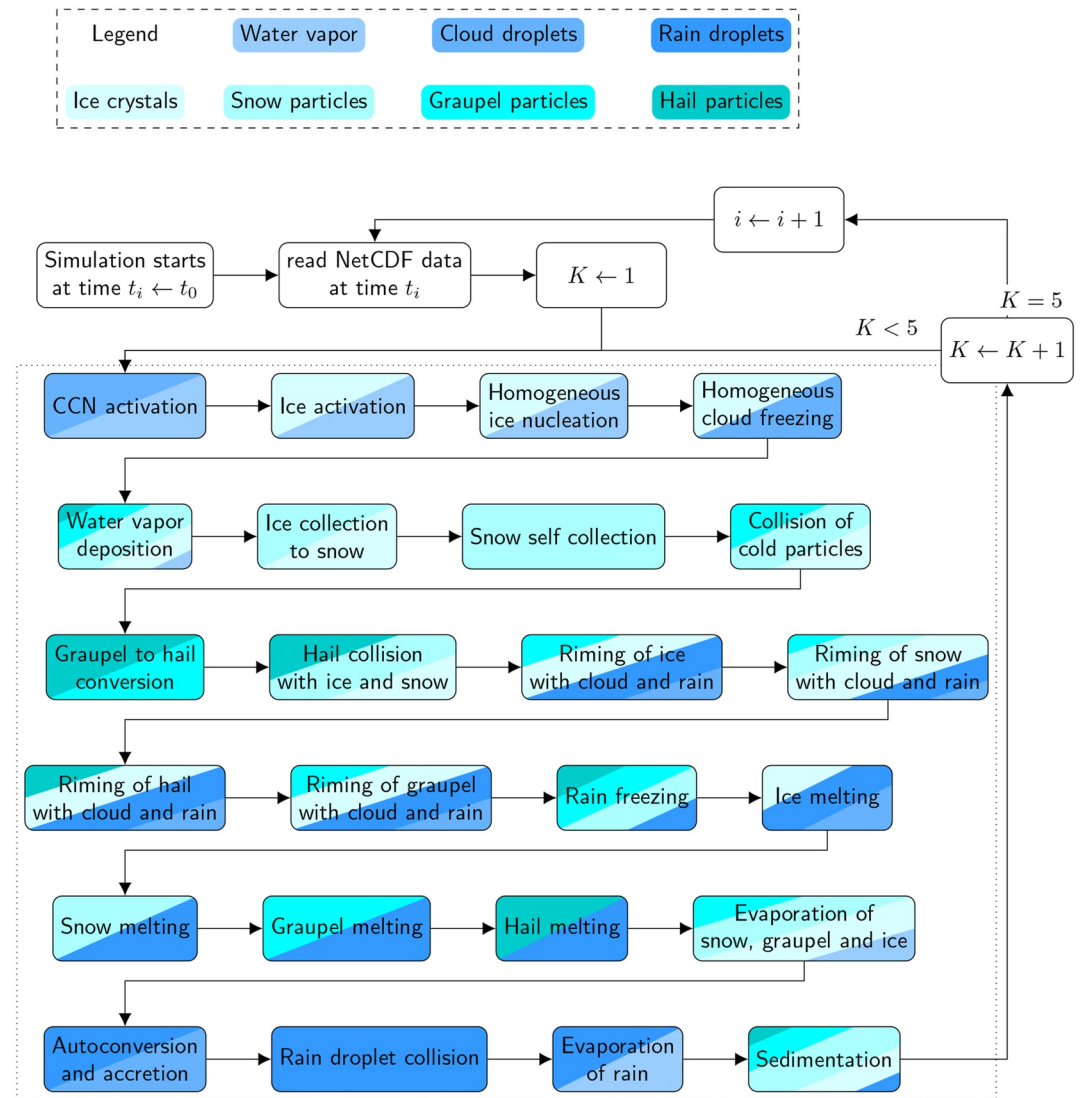


Figure 3. Workflow of the simulation for every Runge-Kutta step K of order four. The colors indicate which mass or number densities are changed in the respective microphysical process. Parallel operator splitting is applied, that is, all processes operate on the same model state in each iteration, and results are gathered at every step. The thermodynamics from precomputed trajectories is read from a NetCDF-file, and used as drivers.

limit of $\Delta t \rightarrow 0$, such that we could trace any unreasonable results to our implementation and rule out our chosen integration scheme as the source for any issues.

The processes are implemented with parallel operator splitting (Barrett et al., 2019). Therefore each process is being evaluated using the same state in the Runge-Kutta substep, and their impact is added to the state at the end of each iteration as outlined in Figure 3. After the microphysical processes are done within a single Runge-Kutta step, we use saturation adjustment (i.e., Asai, 1965; Fisher & Caplan, 1963; Kogan & Martin, 1994; Soong & Ogura, 1973; McDonald, 1963), where we assume that water vapor and cloud droplets are in thermodynamic equilibrium and adjust the temperature accordingly.

We update the thermodynamic variables every time step with the precomputed values from the COSMO simulation. Temperature and pressure changes due to cloud microphysical processes are taken into account within each Runge-Kutta substep. As an example, for a time step from t to $t + \Delta t$, the temperature $T(t)$ and $T(t + \Delta t)$ is

given by the COSMO simulation. For any Runge-Kutta substep, we consider the effect of the microphysics as a function f :

$$f(t, T) = \left. \frac{dT(t)}{dt} \right|_{\text{mphys}} \quad (6)$$

Then the effect is calculated in each substep with:

$$k_1 = f(t, T) \quad (7)$$

$$k_2 = f\left(t + \frac{\Delta t}{2}, T + \Delta t \frac{k_1}{2}\right) \quad (8)$$

$$k_3 = f\left(t + \frac{\Delta t}{2}, T + \Delta t \frac{k_2}{2}\right) \quad (9)$$

$$k_4 = f\left(t + \Delta t, T + \Delta t \cdot k_3\right) \quad (10)$$

The final temperature $T(t + \Delta t)$ is given by the COSMO simulation and not the weighted sum of all changes k_i as usually done for the Runge-Kutta method. The difference between the temperature calculated via the weighted sum and the value given by the COSMO simulation is in $O(10^{-2}\text{K})$ which is the effect of latent heating. This is done analogously for pressure. In addition to updating the thermodynamics at every time step, we add any sedimentation influx as diagnosed from the COSMO simulation to our box, as this depends on the processes in the column above the parcel and hence cannot be calculated from our box-model. In contrast, hydrometeor fluxes out of the parcel due to sedimentation are computed by our box-model.

The cloud microphysical model used for simulations along the pre-calculated WCB trajectories (see Section 2.2) is a re-implementation of the two-moment microphysics as implemented in the Consortium for Small-scale MOdeling (COSMO) model (Baldauf et al., 2011) and Icosahedral Nonhydrostatic (ICON) model (Zängl et al., 2015) and described by Seifert and Beheng (2006a); Seifert and Beheng (2006b). Some differences to the original description by Seifert and Beheng (2006a) and our implementation exist, and these will be explicitly mentioned below. In addition, we use ice multiplication described by Hallett and Mossop (1974) and follow the notation for ice multiplication from Seifert (2002). We implemented heterogeneous ice nucleation as described by Phillips et al. (2008) and homogeneous ice nucleation as described by Kärcher et al. (2006). A complete overview of all parameters and the notation in the corresponding sources is given in the supplementary information.

In a two-moment scheme, one assumes a fixed distribution type and width to describe the particle size distribution of each hydrometeor category. Two moments, which typically are the mass densities in $[\text{kgm}^{-3}]$ and the number densities in $[\text{m}^{-3}]$ (Khain et al., 2015), are the prognostic variables in the scheme. The particle mass distribution $f[\text{m}^{-3} \text{kg}^{-1}]$ is assumed to follow a Γ -distribution of the form (Seifert & Beheng, 2001)

$$f(m) = N_0 m^\mu \exp(-\lambda m^\nu), \quad (11)$$

where m is the mass, N_0 is the intercept, μ is the shape parameter, λ is the slope, and ν is the dispersion parameter.

The n th moment of a distribution f is defined as

$$M^{(n)} = \int_0^\infty m^n f(m) dm, \quad (12)$$

such that for $n = 1$, one gets the mass density over all particle sizes, which is used in one-moment schemes as well, and for $n = 0$, one gets the number density. Mass densities are given for different hydrometeor types $q \in \{Q_{\text{cloud}}, Q_{\text{rain}}, Q_{\text{snow}}, Q_{\text{ice}}, Q_{\text{graupel}}, Q_{\text{hail}}\}$. Overall, two-moment schemes can be more realistic than one-moment schemes (Khain et al., 2015), for example, due to the representation of aerosol effects that decrease the droplet size with an increase in aerosol number density or due to calculating drop density in addition to drop mass in sedimentation processes.

In the following, we outline one process that has been changed compared to the setup used in COSMO and two processes that are most relevant for the discussion of key uncertain parameters in Section 4.2.

The Cloud Condensation Nuclei (CCN) activation differs from the activation method by Seifert and Beheng (2006a) and that used in the COSMO simulation. The parameterization in COSMO uses empirical activation spectra in the form of a power law of saturation. Therefore, one needs to determine the change in saturation with time dS/dt to calculate the activation rate. Assuming that activation is dominated by the vertical velocity w , an approximation of $w\partial S/\partial z$ is used in COSMO. This obviously needs information of the saturation above and below the current grid point. Since our box simulation does not have this information, we use the parameterization by Hande et al. (2016) instead, which has been used in different studies with ICON (e.g., Costa-Surós et al., 2020; Heinze et al., 2017). The parameterization solely depends on the air parcel's vertical velocity w and the pressure p :

$$\text{CCN}(w, p) = A(p) \cdot \arctan(B(p) \cdot \log(w) + C(p)) + D(p). \quad (13)$$

The dependence of aerosol concentrations (and size distribution) on pressure p is parameterized by the following equations:

$$A(p) = a_{\text{ccn},1} \cdot \arctan(b_{\text{ccn},1} \cdot p + c_{\text{ccn},1}) + d_{\text{ccn},1}, \quad (14)$$

$$B(p) = a_{\text{ccn},2} \cdot \arctan(b_{\text{ccn},2} \cdot p + c_{\text{ccn},2}) + d_{\text{ccn},2}, \quad (15)$$

$$C(p) = a_{\text{ccn},3} \cdot \arctan(b_{\text{ccn},3} \cdot p + c_{\text{ccn},3}) + d_{\text{ccn},3}, \quad (16)$$

$$D(p) = a_{\text{ccn},4} \cdot \arctan(b_{\text{ccn},4} \cdot p + c_{\text{ccn},4}) + d_{\text{ccn},4}. \quad (17)$$

The parameters highlighted in Equations 14–17 are key parameters that are discussed in detail in Section 4.2. The parameter $A(p)$ controls the magnitude of CCN, $B(p)$ the shape, and $C(p)$ and $D(p)$ regulate the dependency on vertical velocity and CCN concentration, respectively.

In the following, we discuss some processes that contain important parameters according to our analysis (see Section 4.2). First, heterogeneous freezing of raindrops is represented in the Seifert and Beheng (2006a) cloud microphysics scheme following the parameterization by Bigg (1953). A stochastic model is used where the relative time rate of change of the size distribution is given by

$$\frac{1}{f(Q_{\text{rain}})} \left. \frac{\partial f(Q_{\text{rain}})}{\partial t} \right|_{\text{het}} = -Q_{\text{rain}} J_{\text{het}}(T) \quad (18)$$

with Q_{rain} the mass density of rain droplets and T the temperature of the environment. Bigg (1953) deduced from his experiments that the rate of ice-germ formation is

$$J_{\text{het}}(T) = b_{\text{HET}} \cdot \exp(a_{\text{HET}} \cdot (T_{\text{freeze}} - T) - 1). \quad (19)$$

The change in rain mass and particle number density using Equation 11 and Equation 18 is then

$$\left. \frac{\partial M^{(n)}}{\partial t} \right|_{\text{het}} = -M^{(n+1)} J_{\text{het}}(T). \quad (20)$$

In order to calculate the moment $M^{(n+1)}$ defined in Equation 11, we need to express the intercept and slope of the particle mass distribution by the mass and particle number density with

$$N_0 = \frac{\nu N}{\Gamma\left(\frac{\mu+1}{\nu}\right)} \lambda^{\frac{\mu+1}{\nu}} \quad (21)$$

$$\lambda = \left(\frac{\Gamma\left(\frac{\mu+1}{\nu}\right)}{\Gamma\left(\frac{\mu+2}{\nu}\right)} \bar{m} \right)^{-\nu}, \quad (22)$$

where N is the particle number density and the mean particle mass $\bar{m} = Q/N$ is the quotient of mass and particle number density. Now we can calculate the moments for number density ($n = 0$) and mass density ($n = 1$) for Equation 20 as

$$M^{(1)} = N\bar{m} \quad (23)$$

$$M^{(2)} = \frac{\Gamma\left(\frac{\mu+3}{\nu}\right)}{\Gamma\left(\frac{\nu+1}{\mu}\right)} \cdot \left(\frac{\Gamma\left(\frac{\nu+1}{\mu}\right)}{\Gamma\left(\frac{\nu+2}{\mu}\right)}\right)^2 \cdot N\bar{m}^2. \quad (24)$$

Note that $M^{(2)} = 20 \cdot N\bar{m}^2$ if the Marshall-Palmer distribution for rain droplet size is used, as done in our simulation.

A second important parameterization according to our analysis in Section 4.2 is the representation of sedimentation velocity. The sedimentation velocity is formulated by Seifert (2008) (his Equation (A10)) as

$$v_k = \alpha_{\text{rain}} - \beta_{\text{rain}} \left(1 + \frac{\gamma_{\text{rain}}}{\lambda}\right)^{-(\mu+k+1)} \quad (25)$$

where $k = 0$ is selected to compute the sedimentation velocity for the number density and $k = 3$ for mass densities. The parameter λ denotes the slope and μ the shape of the underlying assumed particle size distribution in Equation 11. The shape parameter μ can be expressed as follows:

$$\mu = \begin{cases} (\nu_{\text{rain}} + 1)/(\text{geo}_{b,\text{rain}}) - 1 & \text{if } Q_{\text{cloud}} \geq Q_{\text{crit}} \\ \mu_{\text{rain},c,0} \cdot \tanh(4 \cdot \mu_{\text{rain},c,2} \cdot \delta D)^{\mu_{\text{rain},c,5}} + \mu_{\text{rain},c,4} & \text{if } Q_{\text{cloud}} < Q_{\text{crit}} \text{ and } D_{\text{rain}} \leq \mu_{\text{rain},c,3} \\ \mu_{\text{rain},c,1} \cdot \tanh(\mu_{\text{rain},c,2} \cdot \delta D)^{\mu_{\text{rain},c,5}} + \mu_{\text{rain},c,4} & \text{otherwise} \end{cases} \quad (26)$$

with $\delta D = D_{\text{rain}} - \mu_{\text{rain},c,3}$ and $Q_{\text{crit}} = 10^{-7} \text{ kg} \cdot \text{m}^{-3}$. The formulation of μ depends on the mass of cloud droplets Q_{cloud} and the mean diameter size D_{rain} of rain droplets. We do not apply a sensitivity analysis for parameter $\mu_{\text{rain},c,5} = 2$ but we use it to demonstrate possible pitfalls of applying AD in Appendix C.

Finally, the mean diameter of a hydrometeor is calculated as

$$D = \text{geo}_a \cdot \bar{m}^{\text{geo}_b}. \quad (27)$$

The mean diameter is used, that is, as a threshold and as a parameter for the break-up of large rain droplets, for riming of cloud or rain droplets, or conversion of graupel to hail. See the supplementary information for an extensive list of all parameters.

Our re-implementation of the cloud microphysics is slightly different from COSMO, which bears the question of how different the simulation is. We present in Figure 4 a comparison of our simulation and the data from COSMO for four randomly selected trajectories from our data set for specific humidity, liquid and frozen water content, and snow mass density. Even though we switched the CCN activation to a different formulation, hydrometeors are formed at similar time steps, and the magnitude of different hydrometeor mass densities is the same. This shows that the simulation with our implementation is reasonable, although the results can be transferred to COSMO only to a certain degree. An exact recreation of COSMO is not needed but rather a realistic, nonidealized simulation in order to show how AD can help to identify and to quantify important parameters.

3. Estimation of Cloud Microphysics Uncertainties

In order to validate the gradients calculated with AD, we use these to linearly predict the deviation of a simulation if the corresponding parameter was perturbed in Section 3.1. In addition, we evaluate the spread of ensemble simulations with perturbed parameters in Section 3.2. At last, we describe how we use Spearman's rank correlation in Section 3.3 to check for a nonlinear correlation between AD-estimated deviations and ensemble-estimated deviations.

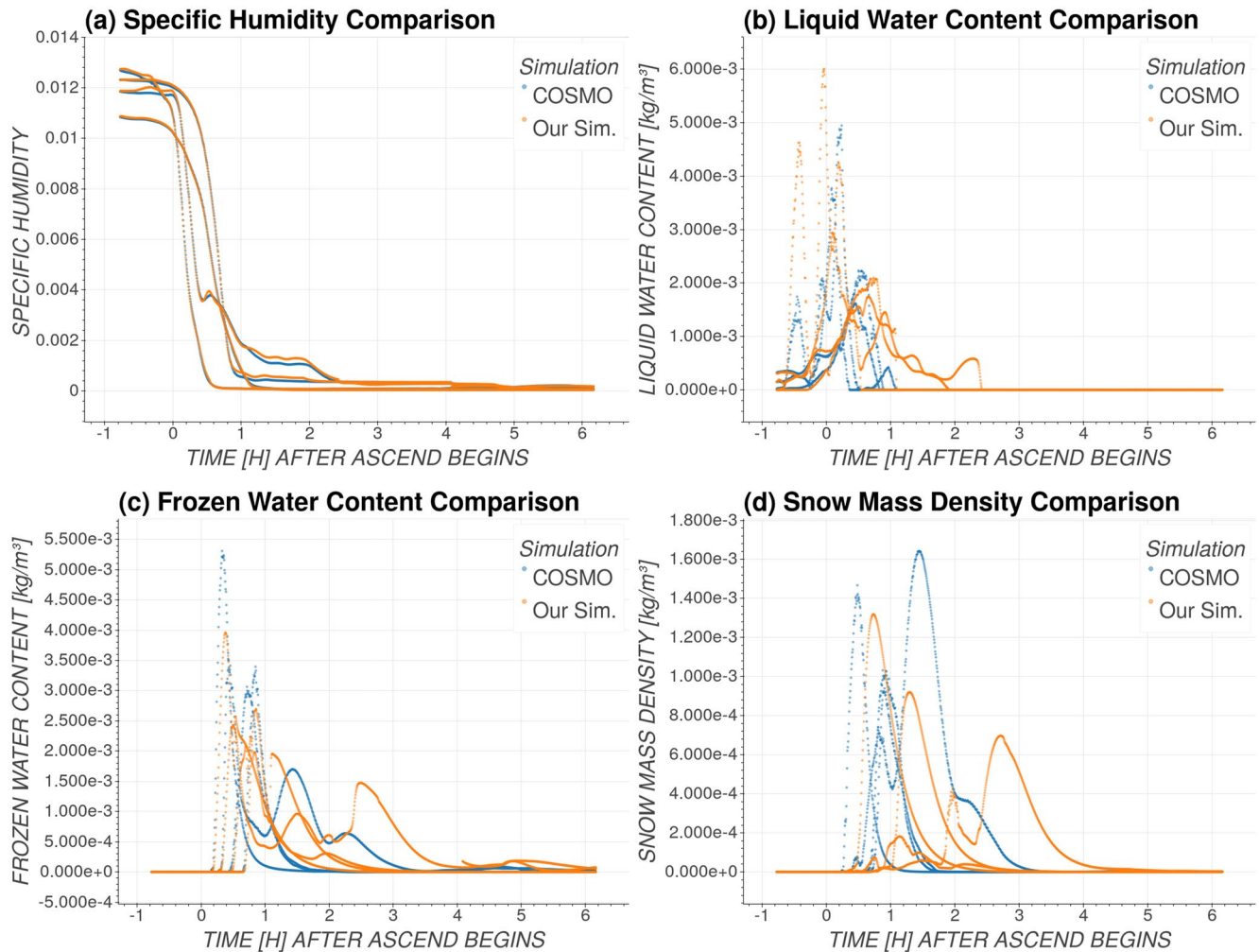


Figure 4. Comparison of the cloud microphysical evolution as simulated by our box-model (orange) and simulated in the COSMO model (blue). Results are shown for four randomly selected trajectories from the complete data set, where two achieve a convective 400 hPa ascent, and the other two achieve a convective 600 hPa ascent. Panel (a) shows the specific humidity, (b) the cloud and rain droplet mass densities, (c) the sum of ice, snow, graupel, and hail, and (d) snow mass density.

3.1. From Sensitivity to Predicted Mean Squared Deviation

Using AD, we can calculate gradients at every time step for every model state variable with respect to every model parameter. These gradients differ in size depending on their impact and the magnitude of the involved model state variable. In order to quantify only the impact of parameters, we formulate a predicted deviation based on the gradients that are averaged over all time steps and trajectories. It is not always possible within an existing cloud microphysics parameterization to represent all interconnections between processes, not least because many parameter values are a result of previous tuning experiments, where parameter interdependencies were considered but are not explicitly formulated in the parameterization equations. Our main purpose for the analysis is to identify parameters and processes with a large impact on cloud property forecasting. If such a parameter is coupled to another parameter which is not found with our approach since the second parameter only has a minor impact on the results, the major impact of the first parameter is not negated. Therefore, we consciously postpone the inclusion of such nonlinear relationships to a further study.

First, we gather data by evaluating gradients for all model state variables listed in Table 1 at every time step, with respect to each model parameter as outlined in Equation 5. Thus, we evaluate

$$\frac{\partial y_s}{\partial x_p} = \frac{\partial \mathcal{M}}{\partial x_p}(x)^T e_s \quad \text{for all } p = 1, \dots, n_{in} \text{ and } s = 1, \dots, n_{out}, \quad (28)$$

where the adjoint direction is given by e_s , and the p th model parameter of \mathcal{M} is denoted by x_p . Note that we use the adjoint derivative since we track sensitivities for far more input parameters than there are output parameters with $177 = n_{\text{in}} \gg n_{\text{out}} = 23$. A table of all 177 input parameters is given as supplementary information (Table S1).

We store these snapshots of all sensitivities for every simulated time step in NetCDF-4 files, which can be used for further analysis.

These sensitivities can be seen as the estimated impact a perturbed model parameter has on a model state variable in the considered time step. In order to identify the most important parameters, we use the sensitivities computed by AD. We predict the deviation of the given model state variable $y_s^{(i,j)}$ at trajectory j and time step i using an Euler integration step perturbing the model parameter x_p by 10% compared to the unperturbed parameter value:

$$D_{\text{pred}}(y_s, x_p) = \frac{\partial y_s^{(i,j)}}{\partial x_p} \cdot 0.1 \cdot x_p \quad (29)$$

The 10% perturbation represents the uncertainty inherent in a given parameter and could be adapted to represent different levels of uncertainty in the value of the various parameters in future work. Here, we use 10% to scale the perturbation for all model parameters, as it is not possible to objectively determine the uncertainty of all 177 investigated model parameters.

The predicted mean squared deviation over all time steps and over all n_{traj} representative trajectories for the model state variable y_s by theoretically perturbing the model parameter x_p by 10% of its original parameter value is

$$\text{MSD}_{\text{pred}}(y_s, x_p) = \frac{1}{n_{\text{time}} \cdot n_{\text{traj}}} \cdot \sum_{j=1}^{n_{\text{traj}}} \sum_{i=1}^{n_{\text{time}}} (D_{\text{pred}}(y_s, x_p))^2. \quad (30)$$

In this equation, n_{time} is the number of simulated time steps. Model parameters with low values of MSD_{pred} for a given model state variable y_s have a low impact over all time steps on this model state variable. Perturbing parameters with low MSD_{pred} for all model state variables would have a minuscule effect on the simulation. Parameters with a large value of MSD_{pred} for any model state variable have a high impact on the simulation, such that perturbations would change the model state variables notably. The MSD_{pred} , according to Equation 30, has been computed for the six representative trajectories (see Section 2.2 for the selection criteria). Each trajectory is simulated with a time step of $\Delta t = 20$ s from $-2,800$ s $= -46.67$ min $\leq t \leq 26,000$ s $= 433.33$ min (relative to the start of the ascend). We use 30 min as spin-up time for our simulation, where we discard the collected data to avoid any initial bias that might be present in the COSMO data from its initialization. The results using MSD_{pred} to find key parameters are discussed in Section 4.2.

MSD_{pred} has two drawbacks in the context of physical consistency: (a) we predict deviations by perturbing parameters independently, although model parameters do have physical relations, for example, the terminal fall velocity of a rain droplet is closely related to its size and shape. (b) We perturb every parameter by a fixed percentage, even though some parameters might have a more narrow validity range, while for others, a larger perturbation factor could be used. These arguments nevertheless do not interfere with our analysis since we want to show the meaningfulness of the gradients given by AD and the overall impact of model parameters compared to each other. It is planned in future work to include physical relations between the model parameters.

3.2. Estimating Uncertainty of Cloud Microphysics With Ensemble Simulations

Since the AD-computed sensitivity is by definition specific to the time step at hand, it is a priori unclear if the sensitivity will attain similar large values at the following time steps. As an example, consider a dissipating cloud with only a few cloud droplets left but a huge number of rain drops. In this situation, the number of cloud droplets is very sensitive to the accretion rate parameter since this parameter describes the rate at which cloud droplets are collected by rain. A slight increase of that parameter for the next time step could result in a complete collection of all remaining cloud droplets by rain drops, rendering this parameter completely irrelevant for subsequent time steps.

To investigate if the AD-derived sensitivities have any meaning beyond the investigated time step, we define a mean squared deviation based on the results of ensemble simulations. This is complementary to $\text{MSD}_{\text{pred}}(y_s, x_p)$,

which is a theoretical deviation of a simulation if a model parameter x_p was perturbed by 10% based on AD. In order to get a comparable measurement to the predicted deviation by perturbing a parameter at an arbitrary time step, we start ensemble simulations for every parameter x_p with $l = 64$ members each at $t = -1,000$ s = -16.67 min before the ascend starts. These are $n_{\text{traj}} \cdot l \cdot 64 = 6 \cdot 177 \cdot 64 = 67,968$ simulations with perturbed parameters. The model state and environment variables are reset to the initial, unperturbed trajectory every 30 min. Applying SPP or any other sophisticated perturbation scheme would require fine-tuning for hundreds of parameters which is out of scope for this paper. Therefore, we apply a simple perturbation scheme as baseline. As a consequence, our sensitivity analysis is about the overall impact of model parameters. In contrast, a more detailed uncertainty analysis would have to incorporate the uncertainty of each model parameter, which may be assessed with different sampling distributions. From the point of view of tuning model parameters, our approach can underestimate the potential of a parameter if 10% is lower than the possible range of a given parameter. The potential changes to prognostic variables is overestimated if 10% is larger than the uncertainty of a model parameter.

By running the simulations for a longer but limited time, the ensembles will not be too far off from the unperturbed trajectory, such that sensitivities from the original trajectory apply to a certain degree to the perturbed ensemble even in later time steps and the state variables of the ensemble members can be compared in a meaningful way. Given the nonlinearity of the cloud scheme, a large perturbation, for example, 10% of a parameter, has the ability to trigger other cloud processes compared to the unperturbed run. If such a situation occurs, then the temporal evolution of the cloud changes in a nonlinear way, where AD-estimated deviations based on an Euler-step may have little meaning. To cover not only nonlinear deviations based on large deviations but also minor effects upon small perturbations, for example, 1% of a parameter, we use a random perturbation. In every ensemble, we perturb exactly one parameter x_p , using the uniform distribution \mathcal{U} (lower, upper)

$$\tilde{x}_p = \mathcal{U}(x_p \cdot 0.9, x_p \cdot 1.1), \quad (31)$$

where \tilde{x}_p denotes the perturbed parameter. Analogous to the formulation in Equation 30, we can define the mean squared deviation for our ensembles as

$$\text{MSD}(y_s, x_p) = \frac{1}{n_{\text{time}} \cdot n_{\text{traj}} \cdot l} \cdot \sum_{j=1}^{n_{\text{traj}}} \sum_{k=1}^l \sum_{i=1}^{n_{\text{time}}} (y_s^{(i,j)} - \tilde{y}_s^{(i,j,k,p)})^2, \quad (32)$$

with n_{time} the number of simulated steps, $y_s^{(i,j)}$ the model state variable y_s at the unperturbed trajectory j and time step i . In this equation, $\tilde{y}_s^{(i,j,k,p)}$ denotes the model state variable y_s of the k th perturbed ensemble member at time step i , with $k = 1, \dots, l$ perturbed parameter values of parameter x_p . As stated in Section 3.1, we do not respect the coupling of model parameters where perturbing one parameter should affect another parameter but rather use these deviations as proof of how AD predicts deviations if a single parameter is perturbed.

3.3. Connection of AD- and Ensemble-Derived Sensitivities

In order to evaluate the correlation between predicted deviations and deviations from perturbed ensembles, we calculate Spearman's rank correlation coefficient for every model state parameter y_s with

$$r(y_s) = \frac{\text{cov}(\text{rank}(\text{MSD}_{\text{pred}}(y_s, x_p)), \text{rank}(\text{MSD}(y_s, x_p)))}{\sigma_{\text{rank}(\text{MSD}_{\text{pred}}(y_s, x_p))} \sigma_{\text{rank}(\text{MSD}(y_s, x_p))}} \text{ for all } x_p \in X, \quad (33)$$

where $\sigma_{\text{rank}(\text{MSD}_{\text{pred}}(y_s, x_p))}$ and $\sigma_{\text{rank}(\text{MSD}(y_s, x_p))}$ are the standard deviations of the rank variables. Thereby, we can quantify any nonlinear correlation between the deviation predicted from AD results and the deviation estimated from ensemble simulations. A correlation near zero would indicate that there is little correlation between sensitivities found via AD and those found in the perturbed ensembles. A value of $r(y_s)$ near one or negative one means there is a (non-)linear correlation and perturbing model parameters with a high impact according to AD change the simulation significantly. A parameter with a higher rank has a larger (predicted) impact and is, therefore, useful to identify processes of interest. The usage of rank correlation instead of, for example, Pearson's correlation coefficient is needed because a mapping of evaluations of a local linearization (our gradients) to the spread of ensembles in a nonlinear model is not trivial. Pearson correlation, however, is a measure of linear correlation, whereas ranked correlation can be used to assess the significance of the relation between two rankings.

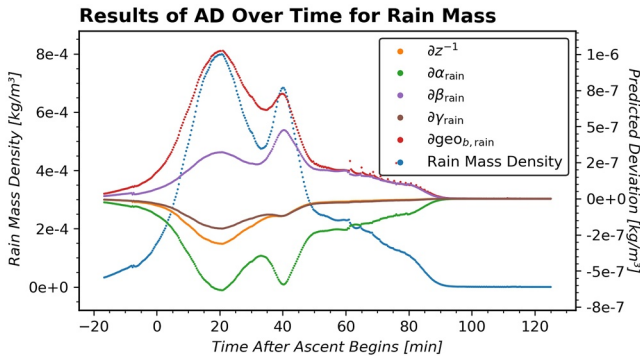


Figure 5. Temporal evolution of rain mass density and AD-estimated deviation for five high-ranking uncertain parameters along the median trajectory rising 600 hPa in about 1.7 hr. Mass density is aligned to the left y-axis, predicted deviation for each model parameter corresponds to the right y-axis.

Filtering small values is a way to improve regular Pearson correlation for our case, but then it relies on how the cutoff for the filtering is determined. Furthermore, predicted deviations tend to overshoot, leading to lower correlation even if the relative impact is correct compared to other parameters. Our main focus in this study is to identify essential parameters and processes and validate their importance relative to each other, which is feasible with ranked correlation. We added Table S2 in the supporting information where we use Pearson's correlation coefficient. However, with the nonlinear correlation, we see correlation values from 0.007 to ≈ 1 for individual model state variables where model parameters with no identified sensitivity have been filtered out. This indicates that Pearson's correlation coefficient is not an appropriate summary of the data since either a lot of data points in the tails are highly linearly correlated (high correlation) or the correlation is not linear (low correlation). A low correlation using Pearson's correlation coefficient can be attributed to outliers but we filtered parameters with no identified sensitivity already out. The high nonlinearity of the model and the drawbacks in the context of physical consistency in our technique explained in Section 3.1 prohibit a ranked correlation of exactly one. We expect AD to predict sensitivities to every model state variable equally well, which would yield similar

correlation values for all model state variables. The strength of the correlation and whether correlation occurs or not are discussed in Section 5.

4. Key Uncertain Cloud Microphysics Parameters

In this section, we use the setup described in Section 2.2 and Section 2.3 with the AD-estimated deviation MSD_{pred} from Section 3.1 for identifying model parameters with the largest overall impact on the cloud microphysical evolution. First, in Section 4.1, we illustrate sensitivities for a single trajectory to show their changes over time. Then, in Section 4.2, the parameters with the largest impact on the cloud microphysical simulation are presented, and the physical plausibility of the results is discussed.

4.1. Sensitivities for a Single Trajectory

The results of the AD algorithm are illustrated with the example of the median trajectory with a convective 600 hPa ascent. We chose this trajectory as an example due to its longer ascent such that any sensitivities might be seen over more time steps compared to the other trajectories considered (see Section 2.2). Figure 5 shows the temporal evolution of rain water mass (blue dots) along with the predicted deviation for five model parameters.

These parameters were selected due to having the largest mean impact over time on the rain mass density out of all 177 parameters considered.

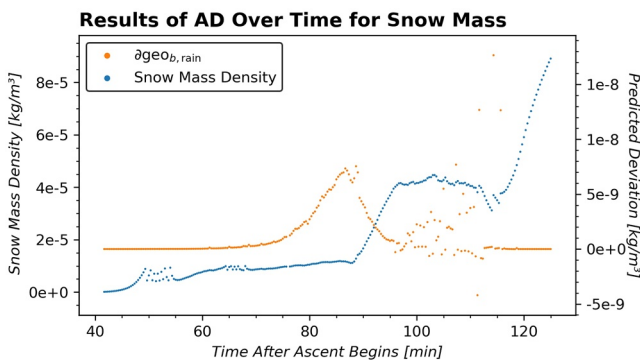


Figure 6. Temporal evolution of snow mass density and AD-estimated deviation upon perturbing $geo_{b,rain}$ by 10% along the median trajectory rising 600 hPa in about 1.7 hr. Mass density is aligned to the left y-axis, AD-estimated deviation corresponds to the right y-axis.

At the start of the ascent, rain mass density rises strongly and decreases quickly around 20 min. After a secondary maximum around 40 min, rain water mass diminishes as the parcel rises and eventually glaciates. The different scales of the rain mass density (left y-axis in Figures 5 and 6) hint at a nonlinear correlation between AD-estimated deviation and deviations from perturbed ensemble simulations. We describe this relationship in detail in Section 5.

Among the identified important model parameters there are $geo_{b,rain}$ (exponent for calculating the mean size of a rain drop), γ_{rain} (exponent for rain sedimentation), α_{rain} (constant in rain sedimentation), and β_{rain} (coefficient in rain sedimentation), which give rise to similar values of AD-estimated deviations and roughly follow the evolution of the rain mass density. These parameters for rain are mainly influencing the removal of rain mass by sedimentation. As in a rising air parcel, sedimentation is one of the key sinks of rain mass,

and sedimentation is proportional to the available rain mass neither the importance of these nor the temporal evolution of their impact is surprising.

Another, albeit more artificial, parameter linked to sedimentation appears in the results: the inverse parcel height z^{-1} . This parameter is reminiscent of the vertical discretization in COSMO. In the context of the microphysics scheme, the parameter corresponds to the discrete grid box in the 3D-model COSMO. The air parcel height directly enters the formulation of the sedimentation fluxes. The relative impact of sedimentation-related parameters decreases with increasing time, that is, as the parcel rises to higher altitudes. This is likely due to the increasing importance of other sink terms in the mixed-phase region of the cloud.

Figure 6 shows the evolution of snow mass density and the AD-estimated deviation upon perturbing $geo_{b,rain}$ by 10%. Similar to the results for rain mass density, $geo_{b,rain}$ has a quite large impact on the snow mass density. The sensitivity is largest in a time window around 80–100 min after the parcel ascent starts, which corresponds to the time interval of rapid glaciation (not shown). At later times little rain water is left (Figure 5), and hence rain freezing has no impact on the further cloud microphysical evolution of the parcel. Also note, that in contrast to the results for rain mass density, AD-estimated deviation for snow mass density does not scale with the mass density itself. This highlights that parameters are not always important throughout the simulation and that sensitivities do not necessarily change smoothly with time, underlining the nonlinearity of the model.

4.2. Key Parameters and Physical Interpretation

In this section, we identify the parameters with the highest impact on microphysics and discuss the implications. Then, we go into detail about how to address uncertainties by providing a (subjective) categorization for each model parameter. We use the term model state variable loosely, where we include sedimentation rates in the model state. To identify the 10 model parameters with the highest AD-estimated deviation for each model state variable as the key uncertain parameters (Table 2), we calculate the mean squared deviation $MSD_{pred}(y_s, x_p)$ from Equation 30 for all model state variables and all 177 model parameters. Since most model parameters are in the top 10 for multiple model state variables, the complete set of key uncertain parameters consists of only 42 distinct parameters, which are listed in Table A1. One might be interested only in the parameters with an effect on the same order of magnitude as the most important parameter. One has to take the nonlinearity of cloud microphysics into account, whereas MSD_{pred} is a linear extrapolation. Predictions for some parameters with a large impact might overshoot, that is, because there is not enough mass to accommodate the perturbation. Therefore, using a wider range is recommended. If we look at two orders of magnitude of the largest MSD_{pred} , the set of parameters coincides mostly with the top 10 parameters as described above. The list of parameters within two orders of magnitude for each parameter adds $geo_{a,graupel}$ and $d_{ccn,3}$ and removes b_{HET} , $x_{rain,min,frz}$, $T_{mult,max}$, and $D_{rainfrz,ig}$. The minimum size of rain droplets $x_{rain,min,frz}$ used in conversion of rain droplets to ice, graupel, and hail, and in homogeneous freezing is in the top 10 list due to its impact on hail. The same is true for the partitioning threshold $D_{rainfrz,ig}$ for freezing rain droplets to hail and for the coefficient b_{HET} for heterogeneous rain freezing. With little hail formation there is sparse data such that these additional parameters may be included with our approach compared to using a threshold. The coefficient $T_{mult,max}$ used for Hallet-Mossop ice multiplication is added to the top 10 parameters list due to its impact on ice number density and sedimentation of ice number, which is just on the edge of being included in the list using two orders of magnitude as cut-off (see Table A1). The additional parameter $d_{ccn,3}$ for CCN activation found by using a cut-off due to its impact on the cloud number is not surprising given that most parameters from CCN activation have a large impact. We already know that this process is important. The geometry parameter $geo_{b,graupel}$ has a large impact on graupel mass density, therefore it is not far-fetched to assume that $geo_{a,graupel}$ is important as well as identified by using a cut-off. All in all, using either a cut-off or the top ten parameters only slightly changes the overall list of identified parameters such that both approaches may be used.

A useful categorization of key uncertain parameters is according to the physical process representation in which they are used. We found six parameters linked to the mass-diameter relationships (“geo” parameters in Table 2) of different hydrometeors, which matches the results of previous studies (e.g., Gilmore et al., 2004; Morales et al., 2018). Seven further parameters are related to the fall velocity-diameter relationships (“vel” parameters in Table 2), which is consistent with other studies (e.g., Forbes & Clark, 2003; Hong et al., 2009; Posselt et al., 2019). Those parameters are used in many process representations, and altered values of these parameters change multiple process rates during a single time step.

A set of influential parameters is associated with the parameterization of rain sedimentation velocity from Equation 25. The formulation of μ in the exponent depends on the number of cloud droplets and the mean diameter size of rain droplets in Equation 26. We identified the parameters ν_{rain} and $\text{geo}_{b,\text{rain}}$ from this equation as key parameters. However, they only matter if the cloud mass density is above the given threshold of $Q_{\text{crit}} = 10^{-7} \text{ kg} \cdot \text{m}^{-3}$. This is expected in our data set of convective ascending air parcels, where cloud formation happens in a short period of time, and the mass of cloud droplets exceeds the threshold early on. Later on, when rain droplets are bigger, the impact of the upper limit of the fall velocity α_{rain} in Equation 25 becomes dominant, which reduces the impact of the parameters of the corresponding case in Equation 26. This relation is mirrored in the AD-estimated sensitivities (see Table A1), where α_{rain} shows the largest impact, closely followed by the coefficient β_{rain} . Next is γ_{rain} , with an AD-estimated deviation of an order of magnitude lower. Furthermore, α_{rain} changes the fall velocity for all sizes in a constant manner, whereas β_{rain} scales the fall velocity for all sizes by a factor determined by μ and γ_{rain} , with the largest impact on light particles.

Finally, an influential process parameterization contributing multiple parameters to the top 10 list of the most influential parameters is the CCN activation. The importance of CCN activation is consistent with previous studies on the impact of aerosol abundance on cloud microphysics (e.g., Carrió et al., 2014; Khain, 2009; Loftus & Cotton, 2014; Tao et al., 2007). The parameterization, according to Hande et al. (2016), contains 16 parameters, which result from an approximation of parcel model simulations for specific vertical profiles of aerosol size distributions. The parameterization captures the vertical velocity w dependence of the CCN activation spectrum and the dependence of aerosol concentrations (and size distribution) on pressure p (compare Equations (13) and (14) to (17)). Eleven of these parameters are found in our list of influential parameters (Table A1): $d_{\text{ccn},3}$, $b_{\text{ccn},3}$, and $d_{\text{ccn},2}$ act on number densities, whereas $c_{\text{ccn},1}$, $a_{\text{ccn},1}$, $b_{\text{ccn},4}$, $c_{\text{ccn},4}$, $b_{\text{ccn},1}$, $d_{\text{ccn},4}$, $a_{\text{ccn},4}$, and $d_{\text{ccn},1}$ act on mass densities. These parameters are highlighted in bold in Equations 14–17. Inspecting Figure 3, only the water vapor, the cloud droplet mass, and the cloud droplet number density are directly influenced by CCN activation. However, AD reveals that the uncertainty in the above parameters also impacts the value of other model state variables by affecting subsequent processes. For example, changes to $d_{\text{ccn},2}$ also change N_{ice} . Note that we listed the model state variable with the highest sensitivity to a given parameter in Table A1. Hence, despite not appearing in Table A1 also water vapor and cloud droplet mass and number density are affected by changes in the CCN activation parameters, albeit with a lower absolute value than by other parameter perturbations.

Given the likely interdependence of the different parameters in the fit, we want to highlight a few interesting aspects instead of discussing one specific parameter: most of our identified eleven parameters are found in the equations for $A(p)$ and $D(p)$, which can be interpreted as representing the absolute number concentration of aerosols at different altitudes in the atmosphere. Perturbing $a_{\text{ccn},1}$, $a_{\text{ccn},4}$, $d_{\text{ccn},1}$, or $d_{\text{ccn},4}$ will change the overall number concentration while altering $b_{\text{ccn},1}$, $b_{\text{ccn},4}$, $c_{\text{ccn},1}$, or $c_{\text{ccn},4}$ modifies the vertical structure of the aerosol number concentration profile. Again, the importance of the aerosol number concentration and its vertical variation is in line with previous studies on the aerosol impact for parcel model simulations. Interestingly, uncertainty in the parameters affecting the absolute aerosol number concentration has the largest impact on ice mass density or ice sedimentation rates, pointing to mixed-phase processes and freezing processes as a consequence of aerosol perturbations. However, for AD to recognize these sensitivities, the ice mass has to be impacted in the same time step as the perturbation in CCN activation. This is only possible if secondary activation is allowed while cloud droplets are freezing in the mixed-phase region of the cloud, which has not been investigated before with WCB trajectories. A more complicated implementation of aerosols taking into account supersaturation and aerosol budgets would be needed to redeem this potentially unphysical behavior. In contrast, the parameters describing the shape of the vertical profile of aerosols act on water vapor as well as cloud and rain water mass, where a direct physical link to CCN activation in a single time step is more plausible, even though rain water mass is not involved in the process. The remaining three influential parameters identified in our analysis act on $B(p)$ and $C(p)$, that is, the vertical velocity dependence of activated CCN. Physically perturbing these would imply changes in the aerosol size distribution (its width or mean diameter) or the chemical aerosol composition at a given pressure level. With the exception of $d_{\text{ccn},2}$, altering their value has the largest impact directly on the cloud droplet number concentration, which is physically meaningful.

So far, we have identified parameters with a large impact and discussed the ramifications. Next, we want to address how to deal with the sensitivities. Ideally, one would like to find constraints on the uncertain parameters in order to reduce the uncertainty inherent in the cloud microphysical scheme. The degree to which this is

possible depends on the nature of the parameter and the available observational or laboratory data. In order to provide guidance on the origin of the parameters, we grouped all model parameters into four possible categories.

1. **Artificial (total 62):** Parameters that have no direct physical meaning or interpretation and are purely needed as a result of parameterizing a process and that are not used as thresholds.
2. **Artificial (Threshold; total 79):** Parameters used as thresholds, sometimes in addition to being parameters in the formulation of a process, are considered artificial since not all real processes act within hard thresholds. Thresholds need to be their own category because AD cannot calculate sensitivities for arguments in if-clauses. However, parameters in this category can be used like normal parameters in addition to thresholds, such that AD may yield a sensitivity (see Section 2.1).
3. **Physical (High Variability; total 27):** Parameters with a physical interpretation but their values need to be considered as highly uncertain either due to uncertainties in observations and measurements or due to the chosen parameterization.
4. **Physical (total 9):** Parameters with a physical interpretation but with less uncertain values compared to the parameters in the latter category.

This categorization of parameters is somewhat subjective and not meant as an ultimate grouping of variables; instead, it is meant to give an idea of the type of the parameter in question and which types are important. From the 42 identified key uncertain parameters, 23 fall into the “artificial” category, 7 are thresholds, 11 belong to the category of “physical” parameters with high variability, and one belongs to the category of physical parameters with low variability.

Even considering that the grouping is the result of expert consultation, such that the total number for each category may vary, we can outline the effect of each on cloud microphysics. With 34 parameters being either artificial or having a high variability, this illustrates that robust estimation of the intrinsic uncertainty of parameters is important for estimating their impact on cloud microphysical uncertainty. For physical parameters with high uncertainty, one should concentrate on making more and more precise measurements to reduce their uncertainty and consequently reduce their impact on the uncertainty of the model state variables. However, since artificial parameters carry sensitivities of comparable magnitudes, these parameters continue to influence the uncertainty of the model state variables even if the physical parameters would be known exactly (e.g., Allen et al., 2003; Palmer et al., 2005; Wilks, 2005). Finding physical constraints for those artificial parameters will be much more challenging or not possible at all.

As an example for an influential, artificial assumption, the artificial parameter a_{HET} for heterogeneous freezing from Equation 19 has the third-largest impact on snow mass density. The underlying assumption is that every ice embryo of equal size that comes from a population of supercooled water droplets has the same probability of reaching the size of a critical embryo (Pruppacher & Klett, 2010). The probability is a result of random fluctuations of water molecules. This leads to the exponential form given in Equation 19 with a_{HET} as a coefficient and b_{HET} as an exponent. This stochastic hypothesis is then fitted against experimental results (e.g., from Barklie & Gokhale, 1959). While experimental errors can be reduced such that the parameter uncertainty in the formulation is reduced, the overall impact of the artificial parameter a_{HET} and therefore of the stochastic hypothesis remains large. If the stochastic hypothesis is not correct or incomplete, then the assumed functional form of Equation 19 is flawed. Such structural uncertainty in the formulation of heterogeneous ice nucleation cannot be reduced with experiments. However, AD helps to identify artificial parameters and accompanying assumptions that have a large impact on the simulation.

A brief summary of the key results from this section: (a) the most influential parameters for the immediate further evolution of the cloud can be determined with AD. (b) The most important process representations involving uncertain parameters are the mass-diameter and fall speed-diameter relationships and the CCN activation. (c) Both directly physically motivated and purely artificial parameters are in the list of most influential parameters identified with AD. (d) Artificial parameter uncertainty may depend on experimental results, which can be improved, and on underlying assumptions of a process, where finding constraints on the uncertainty is more challenging. Note that the grouping of the parameters is based on expert consultation such that the classification is not unambiguous but it gives an idea what kind of questions can arise when investigating a given parameter.

5. The Longer-Time Evolution of Sensitivities

We have demonstrated the use of AD in identifying key uncertain parameters by averaging sensitivities for different model state variables in Section 4. In this section, we investigate the relevance of AD-predicted sensitivities for longer simulation periods by comparing the AD-estimated deviation MSD_{pred} to the ensemble-estimated deviation MSD (e.g., the impact of the maximum size of rain droplets on cloud droplet mass density). The perturbed ensemble parcel model simulations start every 30 min along the baseline parcel trajectory (setup described in Section 3.2). This comparison to ensemble simulations of the longer-term cloud microphysics evolution is important to assess the bearing of instantaneous sensitivities beyond individual time steps. The highly nonlinear nature of cloud microphysics implies that a relation between the two is far from guaranteed.

We present in Figure 7 the relation between AD-estimated deviations and deviations estimated from ensemble simulations for water vapor mass density (a), and (b) zoomed in, and cloud droplet mass density (c) and (d) zoomed in. The x -axis shows the logarithmic AD-estimated mean squared deviation, $\log_{10}(\text{MSD}_{\text{pred}}(Q_{\text{vapor or } Q_{\text{cloud}}}, x_p))$ (Equation 30). The y -axis shows the logarithmic ensemble-estimated mean squared deviation, $\log_{10}(\text{MSD}(Q_{\text{vapor or } Q_{\text{cloud}}}, x_p))$ (Equation 32). Each data point corresponds to the MSD estimates for a certain model parameter x_p . Results are shown separately for the different categories of parameters, that is, artificial, threshold, physical, and highly uncertain physical parameters, introduced in Section 4 (see different colors in Figure 7). The 90% confidence ellipses illustrate the correlation between AD-estimated deviation and ensemble-estimated deviation for all categories except threshold parameters. The range of the two axes is different for two reasons: (a) MSD_{pred} is an estimate of deviation by a perturbation of 10%, whereas MSD is based on random perturbations of up to 10% around the original parameter value. (b) AD-estimates use only gradients with an Euler step, which is not always accurate in a nonlinear model, as discussed in Section 3.2. The figures for the other model state variables have similar shapes to the ones shown for water vapor and cloud droplet mass density with different ranges in the axis and are therefore not shown here but can be found in Figure D1.

To quantify the relation between AD estimated and ensemble estimated sensitivities, we use Spearman's rank correlation coefficient from Equation 33, denoted r in the following. Since the distribution of AD-estimated over ensemble-estimated MSD is similar across all model state variables (Figure 7), we can use r to compare the correlation between each model state variable. Taking all model state variables and model parameters without zero sensitivities according to AD, we get $r = 0.887$, indicating a relatively high ranked correlation. Looking at each model state parameter individually, we can find the same high or even higher correlation coefficients (see the second column of Table 3 for mass densities and the second column of Table B1 for all model state variables) with the exception of sedimentation rates of hail mass and particle number density. For all other state variables, the AD-estimated deviation rank predicts the ensemble-estimated deviation rank with comparable certainty. The lower score for sedimentation rates of hail can be attributed to the very small amount of hail in our simulation.

The aforementioned correlations excluded parameters with zero sensitivity, that is, parameters with no impact on the baseline simulation. Since a perturbation of these parameters might still trigger a process that was initially absent, it makes sense to also include these in the discussion. The correlations taking into account all parameters are shown in the third column of Table 3 and are mostly slightly smaller compared to the values in the second column, where parameters with zero sensitivity are excluded. The difference is small because Spearman's correlation is not very sensitive to outliers on the tails, where few parameters have a high ensemble-estimated deviation and a zero AD-estimated deviation. However, if we consider all parameters for all model state variables together, r becomes much smaller.

The reason for the comparably low correlation is explained in detail in Appendix B. In short, AD-estimated deviation can be arbitrarily small due to an Euler step that is done to estimate the deviation, whereas ensemble-estimated deviation has a minimum for most parameters. This minimum is different for each model state variable, such that low AD-estimated deviations map to different orders of magnitude for ensemble-estimated deviations, which breaks any correlation in this range. A correlation is only visible for parameters with an ensemble-estimated deviation above the minimum. Hence, despite the smaller correlation if all parameters and state variables are considered jointly, the AD-estimated deviations and ensemble-estimated deviations overall agree.

Concerning correlations between AD- and ensemble-estimated deviations for the different parameter categories introduced in Section 4, a clear ranked correlation for all categories except threshold parameters is discernible with the 90% confidence ellipses from Figure 7. Threshold parameters that are used for calculations, as well as the

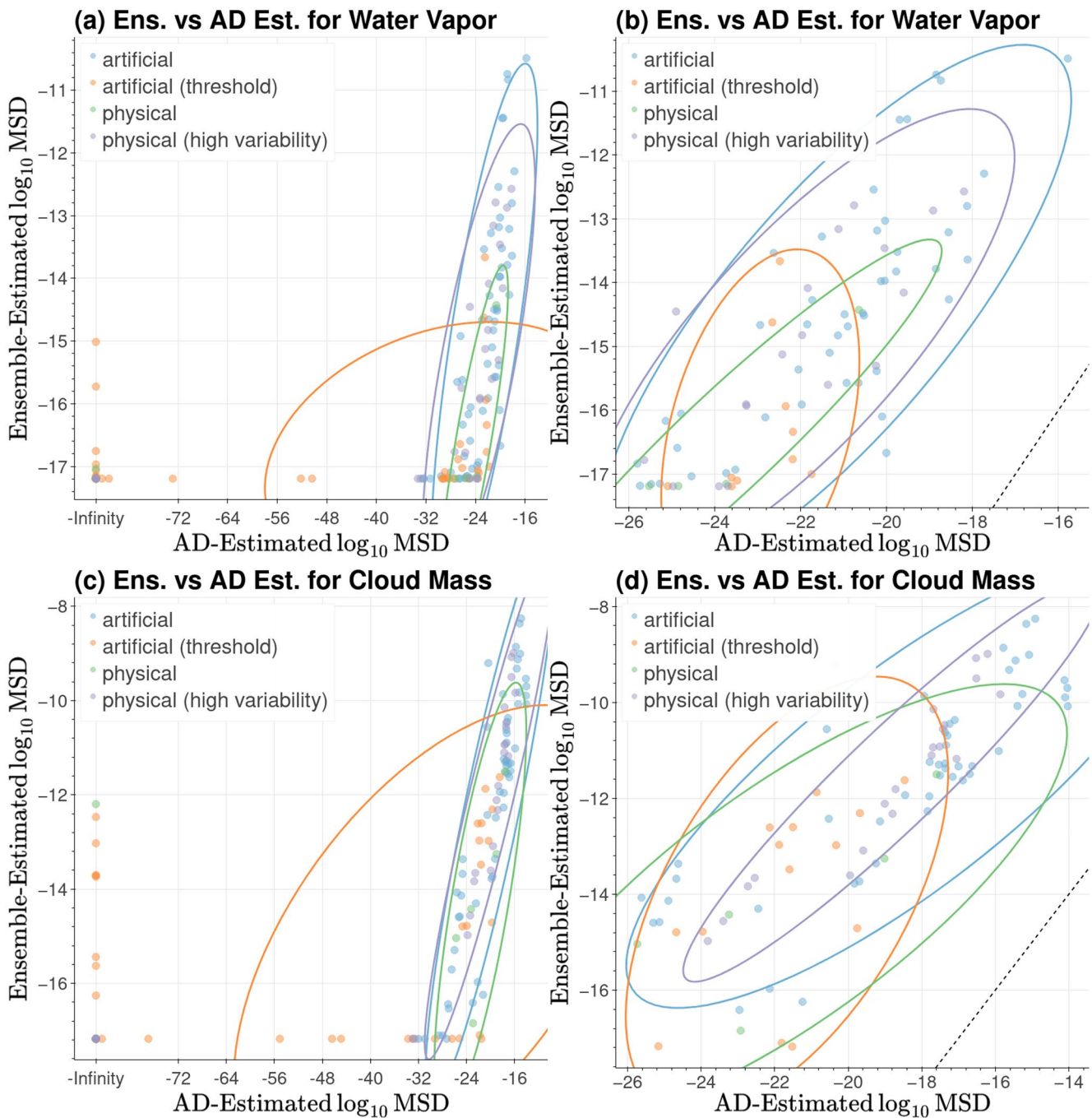


Figure 7. Relation between AD-estimated deviation and ensemble-estimated deviation via perturbing parameters for water vapor (a) and cloud droplet mass density (c). Panels (b), (d) present a zoomed-in version of the right edge of panels (a) and (c), respectively, with a black dashed line representing the 1:1 line. Parameters are below this line if the AD-estimated MSD is larger than the ensemble-estimated MSD and vice versa. Each symbol indicates $MSD_{pred}(Q_{vapor} \text{ or } Q_{cloud}, x_p)$ and $MSD(Q_{vapor} \text{ or } Q_{cloud}, x_p)$ for a specific uncertain parameter x_p . Symbols are color-coded according to the classification into artificial, threshold, and physical parameters with high and low uncertainty introduced in Section 4. In addition, 90% confidence ellipses around data points with AD-estimated deviations above zero are shown for each parameter class.

control flow of the model, cannot easily be evaluated by AD (see Section 2.1). Therefore it is expected that these display a poor correlation between AD-estimated and ensemble-estimated sensitivities. Physical parameters with high variability and artificial parameters can be found on the top right of both plots in Figure 7, which suggests that those parameters contribute the most to model uncertainty. Furthermore, the results presented here confirm

that artificial parameters not used as thresholds and physical parameters with a high variability have a larger impact on the simulation compared to other parameters, see Section 4.2, even on longer timescales.

Given the overall high rank correlation between the AD-estimated deviations, which are based on instantaneous derivatives and linear predictions via an Euler step for a given simulation, and the ensemble-estimated deviations from perturbed ensemble simulations, we can infer that the key parameters found via AD are indeed parameters with a long-term effect on the simulation. The similar rank correlation across most model state variables shows that AD is not limited to few characteristics of a model but can be applied to a wide range of variables and parameters. Parameters that have shown zero sensitivity in AD analysis are an exception since they either influence the control flow or had no impact on the given simulation used in the AD evaluation.

6. Discussion and Summary

This study describes the usage of Algorithmic Differentiation (AD) to assess the impact of 177 uncertain parameters within a two-moment cloud microphysics scheme at once. This study contrasts with numerous other studies which only consider few parameters, mainly fewer than 10.

We emphasize that each model carries two fundamental types of uncertainties:

1. Structural uncertainty,
2. Parametric uncertainty.

Structural uncertainty refers to the structure of the model formulation, for example, the right-hand side of a differential equation. Parameter uncertainty refers to the uncertainty of the model parameters which are present in a chosen formulation. Ideally, this uncertainty should be included in the model using a stochastic representation (Buizza et al., 1999). At best, one would reduce the structural uncertainty by finding new formulations which depend less on artificial parameters, but this may not be feasible due to computational constraints or incomplete physical understanding of the process in question. Structural uncertainty inherent in virtually every subgrid parameterization cannot be unveiled by the use of AD since AD only allows the investigation of implemented code. An interesting idea to approach the structural uncertainty of the cloud model formulations is outlined in Morrison et al. (2020), where Bayesian machine-learning techniques are used to determine the “most probable” structure for the governing differential equation using observational data. However, the more classical approach to formulate the model equation relies on either physical understanding of the processes, constructing a fit curve based on observed or simulated data, or even a mixture of these variants. Uncertain parameters might be present in both approaches, and AD helps to find the most sensitive ones.

We re-simulate the microphysics within air parcels of a warm conveyor belt using the two-moment scheme by Seifert and Beheng (2006a) with CCN activation by Hande et al. (2016) along given WCB trajectories to get realistic thermodynamic parcel evolutions. Therefore, this study does not have a coupling to the flow dynamics and thermodynamic parcel evolution. We limit ourselves to three representative trajectories (25th, 50th, and 75th percentile) for convective trajectories with a 400 hPa ascent within one hour and a 600 hPa ascent within three hours each. These trajectories are associated with the North Atlantic extratropical cyclone “Vladiana” that occurred 22–25 Sep 2016 (Schäfler et al., 2018). By applying AD using CoDiPack (Sagebaum et al., 2018) on the microphysics, we gather the sensitivities of 23 model state variables to 177 model parameters for every time step. Those sensitivities are averaged over six representative trajectories and over all time steps to quantify the overall impact of each model parameter.

We determine the most important parameters through the ranking of their AD-estimated sensitivity on each model state variable. According to AD, the most sensitive parameters have their origins in several physical processes (sedimentation of rain, CCN activation, and heterogeneous freezing) and specific assumed relations (influence of mass on terminal velocity and mass-diameter relations).

The sedimentation velocity of rain droplets is a process featuring multiple parameters with a large impact. The relation of fall velocity-diameter size follows a power law with an upper limit for the fall velocity. This upper limit is the most important parameter in the formulation, followed by the coefficient that scales the fall velocity for different sizes. Parameters in the exponent of the power law depend on the amount of cloud mass and rain droplet size, which are thresholds for different formulations.

We further identified 11 of 16 parameters from CCN activation as key parameters, highlighting the importance of the process. This is consistent with previous studies on the impact of aerosols abundance on cloud microphysics (e.g., Carrió et al., 2014; Khain, 2009; Loftus & Cotton, 2014; Tao et al., 2007). Even though only water vapor and cloud droplets are involved in this process, AD reveals an indirect impact of some parameters to other model state variables through subsequent processes. Most of the identified parameters can be interpreted as representing the absolute number concentration of aerosols at different altitudes in the atmosphere. The parameters affect either the absolute number concentration or the vertical structure of the aerosol number concentration profile.

The nature of the parameter and the available observational or laboratory data determine how much a parameter's uncertainty can be constrained. As a (subjective) guidance, we grouped all model parameters into four possible categories, namely artificial, artificial (threshold), physical (high variability), and physical.

Among the 42 identified important parameters, there are 11 physical parameters with significant uncertainty, such as parameters to calculate the particle velocity or the thermal capacity of ice crystals. Furthermore, there are 23 artificial parameters, that is, parameters for fitted curves as for example, CCN concentrations or coefficients to calculate the diameter of a snowflake. The large number of artificial parameters identified as key parameters might render some artificial assumptions more influential than the precise model physics. Finding physical constraints for such parameters will be much more challenging than for physically motivated parameters or not possible at all.

AD considers instantaneous derivatives of processes with respect to the uncertain parameters. However, it is not clear whether these translate to an impact of a given parameter choice over longer integration times due to the highly nonlinear nature of cloud microphysics. Therefore, we simulated ensembles with one perturbed parameter starting every 30 min along the considered thermodynamic trajectory with an integration time of 30 min. Based on these ensemble simulations, we can estimate the impact of a parameter on a model state variable by perturbing each parameter individually for 30 min intervals. By comparing these changes in model state variables to the expected changes based on AD instantaneous sensitivities averaged over the same time horizon, we found a strong (ranked) correlation between both except for threshold parameters, which are used for the control flow of the simulation. This ranked correlation indicates that parameters with a large impact according to AD also considerably impact a parcel model simulation upon perturbation. Furthermore, the correlation is similar for all analyzed model state variables, implying that AD performs similarly well regardless of which model state variable is investigated.

The key results from this study are as follows:

1. Algorithmic Differentiation can be used to gather sensitivities at every time step for hundreds of parameters at once.
2. The most influential parameters for the immediate further evolution of the cloud can be determined with AD.
3. The most important process representations involving uncertain parameters for our WCB trajectories are the mass-diameter and fall velocity-diameter relationships, the CCN activation, and heterogeneous freezing.
4. Sensitivities at every time step are relevant for more extended simulation periods (at least 30 min).

In order to quantify the uncertainty precisely, future work should include better characterization of the uncertainty ranges of individual parameters and take into account any dependencies between model parameters. Furthermore, the sensitivities of each time step could be used to pinpoint a time step, where creating an ensemble with perturbed parameters has an impact on the longer-time evolution in order to save computation time. Such improvements are achievable since AD gives an objective identification of key uncertain parameters of a model, where the ranking of these parameters is correct even if a longer integration time is taken into account. However, a more detailed understanding of the connection between AD-estimated sensitivities and uncertainty of a forecast is necessary. This can be achieved by exploring the impact of select parameters with a perturbation scheme that has a good probabilistic skill such as SPP. Another improvement can be achieved by implementing a full 3D model, where the effects of interaction to the environment are tracked. We expect to see changes in latent heating in this case, which in turn can affect the buoyancy. This would be more critical for trajectory paths that are not as stable as those from WCBs, for example, case-studies for deep convection would benefit from a 3D environment within a fully time-evolving model.

Appendix A: Most Important Parameters According to AD

Table A1

The Set of Parameters if We Gather the Ten Most Important Ones for Each Model State Variable

Model param.	MSD	MSD _{pred}	Parameter description
Cloud Mass Density			
$b_{ccn,1}$	8.31×10^{-11}	9.36×10^{-15}	Artificial: Parameter for calculating CCN concentration during CCN activation Hande et al. (2016)
$b_{ccn,4}$	2.00×10^{-10}	9.06×10^{-15}	Artificial: Parameter for calculating CCN concentration during CCN activation Hande et al. (2016)
$c_{ccn,1}$	1.27×10^{-10}	7.86×10^{-15}	Artificial: Parameter for calculating CCN concentration during CCN activation Hande et al. (2016)
$c_{ccn,4}$	2.90×10^{-10}	7.61×10^{-15}	Artificial: Parameter for calculating CCN concentration during CCN activation Hande et al. (2016)
$d_{ccn,4}$	5.54×10^{-9}	1.22×10^{-15}	Artificial: Parameter for calculating CCN concentration during CCN activation Hande et al. (2016)
$d_{ccn,1}$	9.82×10^{-10}	8.27×10^{-16}	Artificial: Parameter for calculating CCN concentration during CCN activation Hande et al. (2016)
$a_{ccn,4}$	4.32×10^{-9}	6.94×10^{-16}	Artificial: Parameter for calculating CCN concentration during CCN activation Hande et al. (2016)
k_r	8.41×10^{-11}	4.01×10^{-16}	Artificial: Coefficient for accretion of cloud droplets to rain droplets
$a_{ccn,1}$	7.50×10^{-10}	3.55×10^{-16}	Artificial: Parameter for calculating CCN concentration during CCN activation Hande et al. (2016)
Rain Mass Density			
$geo_{b,rain}$	2.37×10^{-9}	1.26×10^{-13}	Artificial: Exponent for diameter size calculation
α_{rain}	1.68×10^{-9}	4.36×10^{-14}	Physical (High Variability): Constant in rain sedimentation
β_{rain}	9.03×10^{-10}	1.48×10^{-14}	Physical (High Variability): Coefficient for rain sedimentation
z^{-1}	2.14×10^{-10}	9.33×10^{-15}	Artificial: Inverse of air parcel size (height) used in explicit sedimentation
$geo_{a,rain}$	8.59×10^{-11}	4.82×10^{-15}	Artificial: Coefficient for diameter size calculation
Graupel Mass Density			
$vel_{b,rain}$	4.34×10^{-10}	1.87×10^{-14}	Physical (High Variability): Exponent for particle velocity
$vel_{b,graupel}$	2.15×10^{-9}	1.24×10^{-14}	Physical (High Variability): Exponent for particle velocity
$geo_{b,graupel}$	1.60×10^{-10}	6.98×10^{-15}	Artificial: Exponent for diameter size calculation
$vel_{a,rain}$	3.75×10^{-11}	1.31×10^{-15}	Physical (High Variability): Coefficient for particle velocity
$p_{sat,melt}$	4.42×10^{-11}	1.31×10^{-15}	Physical: Saturation pressure at $T = T_{freeze}$
$vel_{a,graupel}$	1.39×10^{-11}	3.77×10^{-16}	Physical (High Variability): Coefficient for particle velocity
Hail Mass Density			
μ_{rain}	1.31×10^{-11}	1.53×10^{-15}	Physical (High Variability): Shape parameter of the generalized Γ -distribution
$x_{rain,min,frz}$	1.64×10^{-18}	3.46×10^{-19}	Artificial (Threshold): Minimum size of particle for freezing
$x_{min,rain}$	1.77×10^{-18}	3.46×10^{-19}	Artificial (Threshold): Minimum size of the particle used in one-moment schemes
$D_{rainfrz,ig}$	7.18×10^{-24}	8.31×10^{-20}	Artificial (Threshold): Size thresholds for partitioning of freezing rain in the hail scheme
Ice Mass Density			
$geo_{b,ice}$	1.21×10^{-9}	4.93×10^{-16}	Artificial: Exponent for diameter size calculation
$vel_{b,ice}$	1.07×10^{-10}	1.29×10^{-17}	Physical (High Variability): Exponent for particle velocity
$v_{ice,sedi,max}$	1.70×10^{-11}	6.51×10^{-18}	Artificial (Threshold): Maximum sedimentation velocity parameter
$geo_{a,ice}$	1.46×10^{-11}	6.13×10^{-18}	Artificial: Coefficient for diameter size calculation

Table A1
Continued

Model param.	MSD	MSD _{pred}	Parameter description
Snow Mass Density			
$geo_{b,snow}$	5.21×10^{-11}	2.58×10^{-16}	Artificial: Exponent for diameter size calculation
a_{HET}	8.84×10^{-12}	1.19×10^{-16}	Artificial: Exponent for rain freeze with data of Barklie and Gokhale
$vel_{b,snow}$	8.50×10^{-13}	8.47×10^{-18}	Physical (High Variability): Exponent for particle velocity
Cloud Droplet Particle Density			
$d_{ccn,3}$	1.83×10^{13}	2.20×10^{13}	Artificial: Parameter for calculating CCN concentration during CCN activation Hande et al. (2016)
$b_{ccn,3}$	1.83×10^{13}	1.46×10^{13}	Artificial: Parameter for calculating CCN concentration during CCN activation Hande et al. (2016)
Hail Particle Density			
b_{HET}	3.94×10^{-10}	1.82×10^{-14}	Artificial: Coefficient for rain freeze with data of Barklie and Gokhale
Ice Particle Density			
$d_{ccn,2}$	1.07×10^{10}	2.29×10^8	Artificial: Parameter for calculating CCN concentration during CCN activation Hande et al. (2016)
$T_{mult,max}$	2.37×10^7	9.85×10^7	Artificial: Coefficient used in Hallet-Mossop ice multiplication
Snow Particle Density			
$D_{rainfrz,gh}$	1.55×10^{-4}	9.22×10^3	Artificial (Threshold): Size thresholds for partitioning of freezing rain in the hail scheme
Sedimentation Of Rain Droplet Mass Density			
γ_{rain}	4.90×10^{-13}	3.82×10^{-15}	Physical (High Variability): Exponent for rain sedimentation
ν_{rain}	3.17×10^{-13}	1.56×10^{-15}	Physical (High Variability): Parameter to calculate the shape of the generalized Γ -distribution
Sedimentation Of Graupel Mass Density			
$v_{graupel,sedi,max}$	3.75×10^{-13}	1.15×10^{-15}	Artificial (Threshold): Maximum sedimentation velocity parameter
ρ_{vel}	1.46×10^{-14}	5.65×10^{-17}	Artificial: Exponent for density correction
Sedimentation Of Snow Crystal Mass Density			
$v_{snow,sedi,max}$	4.99×10^{-16}	3.32×10^{-19}	Artificial (Threshold): Maximum sedimentation velocity parameter

Note. Equation 30 defines the AD-estimated MSD_{pred}, where we only show the highest AD-estimated deviation among all mass densities unless the parameter did not impact mass densities. In that case, the AD-estimated deviation on number density and precipitation is considered. There are 42 different parameters in total.

Appendix B: Correlation Between AD-Estimated MSD and Ensemble-Estimated MSD

Table B1

Spearman's Rank Correlation for AD-Estimated Deviation and Ensemble-Estimated Deviation for Every Model State Variable and All Model State Variables Together

Model State Parameter y_s	$r(y_s)$ without zero sensitivities	$r(y_s)$
Water Vapor Mass Density	0.863	0.889
Cloud Mass Density	0.927	0.904
Rain Mass Density	0.901	0.868
Graupel Mass Density	0.900	0.845
Hail Mass Density	0.906	0.818
Ice Mass Density	0.924	0.884
Snow Mass Density	0.864	0.815
Cloud Droplet Particle Density	0.901	0.880

Table B1

Continued

Model State Parameter y_s	$r(y_s)$ without zero sensitivities	$r(y_s)$
Rain Droplet Particle Density	0.942	0.898
Graupel Particle Density	0.855	0.799
Hail Particle Density	0.788	0.617
Ice Particle Density	0.874	0.789
Snow Particle Density	0.850	0.807
Sedimentation of Rain Droplet Mass Density	0.886	0.872
Sedimentation of Graupel Mass Density	0.880	0.845
Sedimentation of Ice Crystal Mass Density	0.920	0.883
Sedimentation of Snow Crystal Mass Density	0.846	0.754
Sedimentation of Rain Droplets	0.917	0.886
Sedimentation of Graupel Particles	0.839	0.813
Sedimentation of Ice Crystals	0.842	0.777
Sedimentation of Snow Crystals	0.791	0.730
All Together	0.887	0.543

Note. The lower correlation in hail is probably due to the overall low amount of hail in the simulation. Sedimentation of hail has not been triggered, therefore there is no correlation to be found.

If we look at the correlation for all parameters together, Spearman's rank correlation coefficient falls to 0.543, where the different magnitudes of outliers influence the coefficient. As an example, we can compare the outliers for cloud droplet mass and number density. Outliers on the left tail for cloud droplet mass density (Figure 7) are data points where the ensemble-estimated deviation does not go below a certain point with

$$\text{MSD}_{\text{pred}}(Q_{\text{cloud}}, x_p) \lesssim 10^{-27} \text{ and } \text{MSD}(Q_{\text{cloud}}, x_p) \approx 10^{-18}. \quad (\text{B1})$$

For cloud number density (not shown), the corresponding values are orders of magnitudes higher with

$$\text{MSD}_{\text{pred}}(N_{\text{cloud}}, x_p) \lesssim 10^{-12} \text{ and } \text{MSD}(N_{\text{cloud}}) \approx 10^3. \quad (\text{B2})$$

To assure that these outliers appear only at the tail, that is, where parameters have a minor effect, we can calculate r for all model state variables but only with parameters x_p with a sufficiently large effect. We define sufficiently large here broader than in Section 4.2 with

$$\text{for all } x_p \text{ there exists } y_s \text{ with } \text{MSD}_{\text{pred}}(y_s, x_p) \geq P_{75}(\text{MSD}_{\text{pred}}(y_s, x)). \quad (\text{B3})$$

$P_{75}(\text{MSD}_{\text{pred}}(y_s, x))$ is the 75th percentile of $\text{MSD}_{\text{pred}}(y_s, x)$ for a given model state variable y_s . We do not include sedimentation of hail for this, since hail sedimentation is never triggered, and therefore all $\text{MSD}_{\text{pred}} = 0$. With these restrictions, we get a set of 99 parameters and a correlation of $r = 0.901$, which is in range with the coefficients for each model state individually. The high correlation indicates that the AD-estimated sensitivities correlate with ensemble-estimated sensitivities for parameters with a large impact rather than with a low impact. Further, it reveals that AD-estimated sensitivities are correctly ranked throughout different model state variables despite the different magnitudes of those variables, such that they can be put in relation to each other.

Appendix C: Possible Pitfall of Applying AD

When applying AD, one must carefully examine the codomain of the model and the sensitivities. As an example, we take a detailed look at the parameter $\mu_{\text{rain},e,5}$. This parameter serves as an example here, it is not a parameter one can use for tuning. It acts as an exponent for calculating the shape parameter μ during rain evaporation. It is an example for a parameter featuring a gradient with complex numbers that can be a source of error for AD analysis, as hinted in Section 2.1. To illustrate the issue in more detail, we demonstrate with a simple example

why the gradient is not always real-valued in this case. Equation 26 describes the relationship between the shape parameter μ and $\mu_{\text{rain},c,5}$, which we can simplify for the case $Q_{\text{cloud}} < Q_{\text{crit}}$ and $D_{\text{rain}} \leq \mu_{\text{rain},c,3}$, and ignoring $\mu_{\text{rain},c,0}$ and $\mu_{\text{rain},c,4}$ to assume a function of the form

$$y = \tanh \left((4 \cdot \mu_{\text{rain},c,2} \cdot (D_{\text{rain}} - \mu_{\text{rain},c,3}))^{\mu_{\text{rain},c,5}} \right). \quad (\text{C1})$$

To see, what any AD algorithm has to calculate, we set

$$\begin{aligned} w_1 &= 4 \cdot \mu_{\text{rain},c,2} \cdot (D_{\text{rain}} - \mu_{\text{rain},c,3}), \\ w_2 &= w_1^{\mu_{\text{rain},c,5}}, \\ y &= \tanh(w_2). \end{aligned} \quad (\text{C2})$$

Applying the chain rule results in

$$\frac{\partial y}{\partial \mu_{\text{rain},c,5}} = \frac{\partial y}{\partial w_2} \frac{\partial w_2}{\partial \mu_{\text{rain},c,5}} = \text{sech}^2(w_2) \cdot w_1^{\mu_{\text{rain},c,5}} \cdot \log(w_1). \quad (\text{C3})$$

But for the case $D_{\text{rain}} < \mu_{\text{rain},c,3}$ we have $w_1 = D_{\text{rain}} - \mu_{\text{rain},c,3} < 0$, and the gradient becomes a truly complex number after taking the logarithm $\log(w_1)$.

This shows a limitation of AD when functions are assumed to have real-valued derivatives or where using complex-valued derivatives is not optimized and therefore not used by default. One can apply custom functions for calculating derivatives with CoDiPack for special cases if the rest of the model is real-valued, but interpreting complex gradients is a problem in itself, as the imaginary part might not have an intuitive or physical meaning. Running the whole model with complex numbers comes at a computational cost, which may not be reasonable if only a single parameter might lead to complex gradients. Further note that Seifert and Beheng (2006a) fixed the value of this parameter to $\mu_{\text{rain},c,5} = 2$, and did not describe it as a parameter for model tuning.

Appendix D: Comparison of AD-Estimation and Ensemble-Estimation

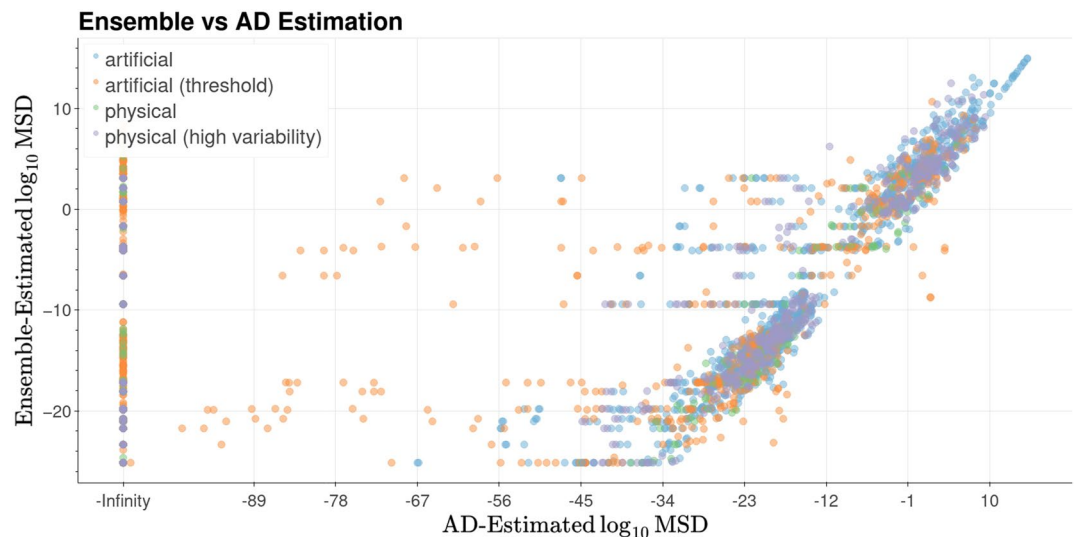


Figure D1. Relation between AD-estimated deviation and ensemble-estimated deviation via perturbing parameters. Each symbol indicates $\text{MSD}_{\text{pred}}(y_s, x_p)$ and $\text{MSD}(y_s, x_p)$ for a specific uncertain parameter x_p and a model state variable y_s . Symbols are color-coded according to the classification into artificial, threshold, and physical parameters with high and low uncertainty introduced in Section 4. The different magnitudes of cloud number and mass density result in the two distinct clusters visible here.

Data Availability Statement

The source code (Algorithmic Differentiation for Sensitivity Analysis in Microphysics v2.2) and the input data with representative trajectories as used in this study are available via Hieronymus (2022). The full set of trajectories is available via iRODS of the Johannes Gutenberg-University Mainz. A script to download the data is given in Hieronymus (2022).

Acknowledgments

Parts of this research were conducted using the supercomputer Mogon II, and auxiliary services offered by Johannes Gutenberg University Mainz (hpc.uni-mainz.de), which is a member of the AHRP and the Gauss Alliance e.V. The authors acknowledge support by the Deutsche Forschungsgemeinschaft (DFG) within the Transregional Collaborative Research Centre TRR165 Waves to Weather (www.wavestoweather.de), Project Z2 as well as funding from JGU Mainz. We would like to thank the reviewers for their valuable and helpful comments. We appreciate their suggestions that led to a significantly improved manuscript. Open Access funding enabled and organized by Projekt DEAL.

References

- Allen, M., Kettleborough, J., & Stainforth, D. (2003). Model error in weather and climate forecasting. In *Seminar on predictability of weather and climate* (Vol. 9–13(september 2002), pp. 275–294). ECMWF.
- Asai, T. (1965). A numerical study of the air-mass transformation over the Japan sea in winter. *Journal of the Meteorological Society of Japan, Ser. II*, 43(1), 1–15. https://doi.org/10.2151/jmsj1965.43.1_1
- Baldauf, M., Seifert, A., Förstner, J., Majewski, D., Raschendorfer, M., & Reinhardt, T. (2011). Operational convective-scale numerical weather prediction with the COSMO model: Description and sensitivities. *Monthly Weather Review*, 139(12), 3887–3905. <https://doi.org/10.1175/MWR-D-10-05013.1>
- Barklie, R. H. D., & Gokhale, N. R. (1959). *The freezing of supercooled water droplets* (Vol. MW-30, pp. 43–64). Stormy Weather Group Scientific Report.
- Barrett, A. I., Wellmann, C., Seifert, A., Hoose, C., Vogel, B., & Kunz, M. (2019). One step at a time: How model time step significantly affects convection-permitting simulations. *Journal of Advances in Modeling Earth Systems*, 11(3), 641–658. <https://doi.org/10.1029/2018MS001418>
- Baumgartner, M., Sagebaum, M., Gauger, N. R., Spichtinger, P., & Brinkmann, A. (2019). Algorithmic differentiation for cloud schemes (IFS cy43r3) using CoDiPack (v1.8.1). *Geoscientific Model Development*, 12(12), 5197–5212. <https://doi.org/10.5194/gmd-12-5197-2019>
- Bigg, E. K. (1953). The supercooling of water. *Proceedings of the Physical Society Section B*, 66(8), 688–694. <https://doi.org/10.1088/0370-1301/66/8/309>
- Bischof, C. H., Pusch, G. D., & Knoesel, R. (1996). Sensitivity analysis of the MM5 weather model using automatic differentiation. *Computers in Physics*, 10(6), 605. <https://doi.org/10.1063/1.168585>
- Büeler, D., & Pfahl, S. (2017). Potential vorticity diagnostics to quantify effects of latent heating in extratropical cyclones. Part i: Methodology. *Journal of the Atmospheric Sciences*, 74(11), 3567–3590. <https://doi.org/10.1175/JAS-D-17-0041.1>
- Buizza, R., Milleer, M., & Palmer, T. N. (1999). Stochastic representation of model uncertainties in the ECMWF ensemble prediction system. *Quarterly Journal of the Royal Meteorological Society*, 125(560), 2887–2908. <https://doi.org/10.1002/qj.49712556006>
- Carrió, G. G., Cotton, W. R., & Loftus, A. (2014). On the response of hailstorms to enhanced CCN concentrations. *Atmospheric Research*, 143, 342–350. <https://doi.org/10.1016/j.atmosres.2014.03.002>
- Chertock, A., Kurganov, A., Lukáčová-Medvid'ová, M., Spichtinger, P., & Wiebe, B. (2019). Stochastic galerkin method for cloud simulation. *Mathematics of Climate and Weather Forecasting*, 5(1), 65–106. <https://doi.org/10.1515/mcwf-2019-0005>
- Christensen, H. M., Lock, S.-J., Moroz, I. M., & Palmer, T. N. (2017). Introducing independent patterns into the stochastically perturbed parameterization tendencies (SPPT) scheme. *Quarterly Journal of the Royal Meteorological Society*, 143(706), 2168–2181. <https://doi.org/10.1002/qj.3075>
- Costa-Surós, M., Sourdeval, O., Acquistapace, C., Baars, H., Carbajal Henken, C., Genz, C., et al. (2020). Detection and attribution of aerosol–cloud interactions in large-domain large-eddy simulations with the ICOSahedral non-hydrostatic model. *Atmospheric Chemistry and Physics*, 20(9), 5657–5678. <https://doi.org/10.5194/acp-20-5657-2020>
- Economou, T. D., Palacios, F., Copeland, S. R., Lukaczyk, T. W., & Alonso, J. J. (2016). SU2: An open-source suite for multiphysics simulation and design. *AIAA Journal*, 54(3), 828–846. <https://doi.org/10.2514/1.J053813>
- Fisher, E. L., & Caplan, P. (1963). An experiment in numerical prediction of fog and stratus. *Journal of the Atmospheric Sciences*, 20(5), 425–437. [https://doi.org/10.1175/1520-0469\(1963\)020<0425:aeinpo>2.0.co;2](https://doi.org/10.1175/1520-0469(1963)020<0425:aeinpo>2.0.co;2)
- Forbes, R. M., & Clark, P. A. (2003). Sensitivity of extratropical cyclone mesoscale structure to the parameterization of ice microphysical processes. *Quarterly Journal of the Royal Meteorological Society*, 129(589), 1123–1148. <https://doi.org/10.1256/qj.01.171>
- Gilmore, M. S., Straka, J. M., & Rasmussen, E. N. (2004). Precipitation uncertainty due to variations in precipitation particle parameters within a simple microphysics scheme. *Monthly Weather Review*, 132(11), 2610–2627. <https://doi.org/10.1175/MWR2810.1>
- Griewank, A., & Walther, A. (2008). *Evaluating derivatives: Principles and techniques of algorithmic differentiation* (2nd ed.). SIAM.
- Hairer, E., & Wanner, G. (1996). *Solving ordinary differential equations II* (Vol. 14). Springer Berlin Heidelberg.
- Hallett, J., & Mossop, S. C. (1974). Production of secondary ice particles during the riming process. *Nature*, 249(5452), 26–28. <https://doi.org/10.1038/249026a0>
- Hande, L. B., Engler, C., Hoose, C., & Tegen, I. (2016). Parameterizing cloud condensation nuclei concentrations during HOPE. *Atmospheric Chemistry and Physics*, 16(18), 12059–12079. <https://doi.org/10.5194/acp-16-12059-2016>
- Hascoet, L., & Pascual, V. (2013). The tapenade automatic differentiation tool: Principles, model, and specification. *ACM Transactions on Mathematical Software*, 39(3), 1–43. <https://doi.org/10.1145/2450153.2450158>
- Heinze, R., Dipankar, A., Henken, C. C., Moseley, C., Sourdeval, O., Trömel, S., et al. (2017). Large-eddy simulations over Germany using ICON: A comprehensive evaluation. *Quarterly Journal of the Royal Meteorological Society*, 143(702), 69–100. <https://doi.org/10.1002/qj.2947>
- Hieronymus, M. (2022). wavestoweather/AD_sensitivity_analysis: V2.2. *Zenodo*. <https://doi.org/10.5281/ZENODO.6645540>
- Hogan, R. J. (2014). Fast reverse-mode automatic differentiation using expression templates in C++. *ACM Transactions on Mathematical Software*, 40(4), 1–16. <https://doi.org/10.1145/2560359>
- Hong, S.-Y., Sunny Lim, K.-S., Kim, J.-H., Jade Lim, J.-O., & Dudhia, J. (2009). Sensitivity study of cloud-resolving convective simulations with WRF using two bulk microphysical parameterizations: Ice-phase microphysics versus sedimentation effects. *Journal of Applied Meteorology and Climatology*, 48(1), 61–76. <https://doi.org/10.1175/2008JAMC1960.1>
- Igel, A. L., & van den Heever, S. C. (2017a). The importance of the shape of cloud droplet size distributions in shallow cumulus clouds. part i: Bin microphysics simulations. *Journal of the Atmospheric Sciences*, 74(1), 249–258. <https://doi.org/10.1175/JAS-D-15-0382.1>
- Igel, A. L., & van den Heever, S. C. (2017b). The importance of the shape of cloud droplet size distributions in shallow cumulus clouds. part II: Bulk microphysics simulations. *Journal of the Atmospheric Sciences*, 74(1), 259–273. <https://doi.org/10.1175/JAS-D-15-0383.1>
- Johnson, J. S., Cui, Z., Lee, L. A., Gosling, J. P., Blyth, A. M., & Carslaw, K. S. (2015). Evaluating uncertainty in convective cloud microphysics using statistical emulation. *Journal of Advances in Modeling Earth Systems*, 7(1), 162–187. <https://doi.org/10.1002/2014MS000383>

- Joos, H., & Forbes, R. M. (2016). Impact of different IFS microphysics on a warm conveyor belt and the downstream flow evolution: Microphysics in a WCB. *Quarterly Journal of the Royal Meteorological Society*, 142(700), 2727–2739. <https://doi.org/10.1002/qj.2863>
- Joos, H., & Wernli, H. (2012). Influence of microphysical processes on the potential vorticity development in a warm conveyor belt: A case-study with the limited-area model COSMO. *Quarterly Journal of the Royal Meteorological Society*, 138(663), 407–418. <https://doi.org/10.1002/qj.934>
- Kärcher, B., Hendricks, J., & Lohmann, U. (2006). Physically based parameterization of cirrus cloud formation for use in global atmospheric models. *Journal of Geophysical Research*, 111(D1), D01205. <https://doi.org/10.1029/2005JD006219>
- Khain, A. P. (2009). Notes on state-of-the-art investigations of aerosol effects on precipitation: A critical review. *Environmental Research Letters*, 4(1), 015004. <https://doi.org/10.1088/1748-9326/4/1/015004>
- Khain, A. P., Beheng, K. D., Heymsfield, A., Korolev, A., Krichak, S. O., Levin, Z., et al. (2015). Representation of microphysical processes in cloud-resolving models: Spectral (bin) microphysics versus bulk parameterization. *Review of Geophysics*, 53(2), 247–322. <https://doi.org/10.1002/2014RG000468>
- Kim, J. G., Hunke, E. C., & Lipscomb, W. H. (2006). A sensitivity-enhanced simulation approach for community climate system model. In V. N. Alexandrov, G. D. van Albeda, P. M. A. Sloot, & J. Dongarra (Eds.), *Computational science – ICCS 2006* (pp. 533–540). Springer Berlin Heidelberg.
- Kogan, Y. L., & Martin, W. J. (1994). Parameterization of bulk condensation in numerical cloud models. *Journal of the Atmospheric Sciences*, 51(12), 1728–1739. [https://doi.org/10.1175/1520-0469\(1994\)051<1728:pobcin>2.0.co;2](https://doi.org/10.1175/1520-0469(1994)051<1728:pobcin>2.0.co;2)
- Lang, S. T. K., Lock, S., Leutbecher, M., Bechtold, P., & Forbes, R. M. (2021). Revision of the stochastically perturbed parameterisations model uncertainty scheme in the integrated forecasting system. *Quarterly Journal of the Royal Meteorological Society*, 147(735), 1364–1381. <https://doi.org/10.1002/qj.3978>
- Leutbecher, M., Lock, S., Ollinaho, P., Lang, S. T. K., Balsamo, G., Bechtold, P., et al. (2017). Stochastic representations of model uncertainties at ECMWF: State of the art and future vision. *Quarterly Journal of the Royal Meteorological Society*, 143(707), 2315–2339. <https://doi.org/10.1002/qj.3094>
- Loftus, A., & Cotton, W. (2014). Examination of CCN impacts on hail in a simulated supercell storm with triple-moment hail bulk microphysics. *Atmospheric Research*, 147–148, 183–204. <https://doi.org/10.1016/j.atmosres.2014.04.017>
- Madonna, E., Wernli, H., Joos, H., & Martius, O. (2014). Warm conveyor belts in the ERA-interim dataset (1979–2010). part i: Climatology and potential vorticity evolution. *Journal of Climate*, 27(1), 3–26. <https://doi.org/10.1175/JCLI-D-12-00720.1>
- Margossian, C. C. (2019). A review of automatic differentiation and its efficient implementation. *Wiley interdisciplinary reviews: data mining and knowledge discovery*, 9(4). <https://doi.org/10.1002/widm.1305>
- McDonald, J. (1963). The saturation adjustment in numerical modelling of fog. *Journal of the Atmospheric Sciences*, 20(5), 476–478. [https://doi.org/10.1175/1520-0469\(1963\)020<0476:tsainm>2.0.co;2](https://doi.org/10.1175/1520-0469(1963)020<0476:tsainm>2.0.co;2)
- Miltenberger, A. K., Pfahl, S., & Wernli, H. (2013). An online trajectory module (version 1.0) for the nonhydrostatic numerical weather prediction model COSMO. *Geoscientific Model Development*, 6(6), 1989–2004. <https://doi.org/10.5194/gmd-6-1989-2013>
- Morales, A., Morrison, H., & Posselt, D. J. (2018). Orographic precipitation response to microphysical parameter perturbations for idealized moist nearly neutral flow. *Journal of the Atmospheric Sciences*, 75(6), 1933–1953. <https://doi.org/10.1175/JAS-D-17-0389.1>
- Morris, M. D. (1991). Factorial sampling plans for preliminary computational experiments. *Technometrics*, 33(2), 161–174. <https://doi.org/10.1080/00401706.1991.10484804>
- Morrison, H., Lier-Walqui, M., Kumjian, M. R., & Prat, O. P. (2020). A bayesian approach for statistical–physical bulk parameterization of rain microphysics. part i: Scheme description. *Journal of the Atmospheric Sciences*, 77(3), 1019–1041. <https://doi.org/10.1175/JAS-D-19-0070.1>
- Oakley, J. E., & O’Hagan, A. (2004). Probabilistic sensitivity analysis of complex models: A bayesian approach. *Journal of the Royal Statistical Society B*, 66(3), 751–769. <https://doi.org/10.1111/j.1467-9868.2004.05304.x>
- Oertel, A., Boettcher, M., Joos, H., Sprenger, M., Konow, H., Hagen, M., & Wernli, H. (2019). Convective activity in an extratropical cyclone and its warm conveyor belt – A case-study combining observations and a convection-permitting model simulation. *Quarterly Journal of the Royal Meteorological Society*, 145(721), 1406–1426. <https://doi.org/10.1002/qj.3500>
- Oertel, A., Boettcher, M., Joos, H., Sprenger, M., & Wernli, H. (2020). Potential vorticity structure of embedded convection in a warm conveyor belt and its relevance for large-scale dynamics. *Weather and Climate Dynamics*, 1(1), 127–153. <https://doi.org/10.5194/wcd-1-127-2020>
- Ollinaho, P., Lock, S.-J., Leutbecher, M., Bechtold, P., Beljaars, A., Bozzo, A., et al. (2017). Towards process-level representation of model uncertainties: Stochastically perturbed parameterizations in the ECMWF ensemble. *Quarterly Journal of the Royal Meteorological Society*, 143(702), 408–422. <https://doi.org/10.1002/qj.2931>
- Palmer, T. N., Buizza, R., Doblas-Reyes, F., Jung, T., Leutbecher, M., Shutts, G. J., et al. (2009). Stochastic parametrization and model uncertainty. *ECMWF Technical Memoranda*, 598, 1–42. <https://doi.org/10.21957/ps8gbwbdv>
- Palmer, T. N., Shutts, G., Hagedorn, R., Doblas-Reyes, F., Jung, T., & Leutbecher, M. (2005). Representing model uncertainty in weather and climate prediction. *Annual Review of Earth and Planetary Sciences*, 33(1), 163–193. <https://doi.org/10.1146/annurev.earth.33.092203.122552>
- Paszke, A., Gross, S., Massa, F., Lerer, A., Bradbury, J., Chanan, G., et al. (2019). PyTorch: An imperative style, high-performance deep learning library. In H. Wallach, H. Larochelle, A. Beygelzimer, F. D. Alché-Buc, E. Fox, & R. Garnett (Eds.), *Advances in neural information processing systems*. Curran Associates, Inc. (Vol. 32, pp. 8024–8035).
- Phillips, V. T. J., DeMott, P. J., & Andronache, C. (2008). An empirical parameterization of heterogeneous ice nucleation for multiple chemical species of aerosol. *Journal of the Atmospheric Sciences*, 65(9), 2757–2783. <https://doi.org/10.1175/2007JAS2546.1>
- Posselt, D. J., He, F., Bukowski, J., & Reid, J. S. (2019). On the relative sensitivity of a tropical deep convective storm to changes in environment and cloud microphysical parameters. *Journal of the Atmospheric Sciences*, 76(4), 1163–1185. <https://doi.org/10.1175/JAS-D-18-0181.1>
- Pruppacher, H., & Klett, J. (2010). *Microphysics of clouds and precipitation* (2nd ed., Vol. 18). Springer Netherlands.
- Regayre, L. A., Pringle, K. J., Booth, B. B. B., Lee, L. A., Mann, G. W., Browse, J., et al. (2014). Uncertainty in the magnitude of aerosol-cloud radiative forcing over recent decades. *Geophysical Research Letters*, 41(24), 9040–9049. <https://doi.org/10.1002/2014GL062029>
- Sagebaum, M., Albring, T., & Gauger, N. R. (2018). Expression templates for primal value taping in the reverse mode of algorithmic differentiation. *Optimization Methods and Software*, 33(4), 1207–1231. <https://doi.org/10.1080/10556788.2018.1471140>
- Sagebaum, M., Albring, T., & Gauger, N. R. (2019). High-performance derivative computations using CoDiPack. *ACM Transactions on Mathematical Software*, 45(4), 1–26. <https://doi.org/10.1145/3356900>
- Schäfler, A., Craig, G., Wernli, H., Arbogast, P., Doyle, J. D., McTaggart-Cowan, R., et al. (2018). The north atlantic waveguide and downstream impact experiment. *Bulletin American Meteorology Social*, 99(8), 1607–1637. <https://doi.org/10.1175/BAMS-D-17-0003.1>
- Schlenkrich, S., Walther, A., Gauger, N. R., & Heinrich, R. (2008). Differentiating fixed point iterations with ADOL-c: Gradient calculation for fluid dynamics. In H. G. Bock, E. Kostina, H. X. Phu, & R. Rannacher (Eds.), *Modeling, simulation and optimization of complex processes* (pp. 499–508). Springer Berlin Heidelberg.

- Seifert, A. (2002). *Parametrisierung wolkenmikrophysikalischer prozesse und simulation konvektiver mischwolken*, (Ph. D. thesis). Karlsruhe Institute of Technology. (in German) .
- Seifert, A. (2008). On the parameterization of evaporation of raindrops as simulated by a one-dimensional rainshaft model. *Journal of the Atmospheric Sciences*, 65(11), 3608–3619. <https://doi.org/10.1175/2008JAS2586.1>
- Seifert, A., & Beheng, K. D. (2001). A double-moment parameterization for simulating autoconversion, accretion and selfcollection. *Atmospheric Research*, 59–60, 265–281. [https://doi.org/10.1016/S0169-8095\(01\)00126-0](https://doi.org/10.1016/S0169-8095(01)00126-0)
- Seifert, A., & Beheng, K. D. (2006a). A two-moment cloud microphysics parameterization for mixed-phase clouds. part 1: Model description. *Meteorology and Atmospheric Physics*, 92(1), 45–66. <https://doi.org/10.1007/s00703-005-0112-4>
- Seifert, A., & Beheng, K. D. (2006b). A two-moment cloud microphysics parameterization for mixed-phase clouds. part 2: Maritime vs. continental deep convective storms. *Meteorology and Atmospheric Physics*, 92(1), 67–82. <https://doi.org/10.1007/s00703-005-0113-3>
- Soong, S.-T., & Ogura, Y. (1973). A comparison between axisymmetric and slab-symmetric cumulus cloud models. *Journal of the Atmospheric Sciences*, 30(5), 879–893. [https://doi.org/10.1175/1520-0469\(1973\)030<0879:acbaas>2.0.co;2](https://doi.org/10.1175/1520-0469(1973)030<0879:acbaas>2.0.co;2)
- Talnikar, C., & Wang, Q. (2019). A two-level computational graph method for the adjoint of a finite volume based compressible unsteady flow solver. *Parallel Computing*, 81, 68–84. <https://doi.org/10.1016/j.parco.2018.12.001>
- Tao, W.-K., Li, X., Khain, A., Matsui, T., Lang, S., & Simpson, J. (2007). Role of atmospheric aerosol concentration on deep convective precipitation: Cloud-resolving model simulations. *Journal of Geophysical Research*, 112(D24), D24S18. <https://doi.org/10.1029/2007JD008728>
- Veldhuizen, T. (1995). Expression templates. *C++ Report*, 7, 26–31.
- Wellmann, C., Barrett, A. I., Johnson, J. S., Kunz, M., Vogel, B., Carslaw, K. S., & Hoose, C. (2018). Using emulators to understand the sensitivity of deep convective clouds and hail to environmental conditions. *Journal of Advances in Modeling Earth Systems*, 10(12), 3103–3122. <https://doi.org/10.1029/2018MS001465>
- Wernli, H. (1997). A Lagrangian-based analysis of extratropical cyclones. II: A detailed case-study. *Quarterly Journal of the Royal Meteorological Society*, 123(542), 1677–1706. <https://doi.org/10.1002/qj.49712354211>
- Wilks, D. S. (2005). Effects of stochastic parametrizations in the Lorenz '96 system. *Quarterly Journal of the Royal Meteorological Society*, 131(606), 389–407. <https://doi.org/10.1256/qj.04.03>
- Zängl, G., Reinert, D., Ripodas, P., & Baldauf, M. (2015). The ICON (ICOsahedral non-hydrostatic) modelling framework of DWD and MPI-m: Description of the non-hydrostatic dynamical core. *Quarterly Journal of the Royal Meteorological Society*, 141(687), 563–579. <https://doi.org/10.1002/qj.2378>